

University Degree in Biomedical Engineering

Academic Year 2018 - 2019

Bachelor Thesis

“Stiffness study of cancer cells by osmotic shocks”

Chaymaa Zougari Ben El Khyat

Tutors

Álvaro Cano Tortajada

Javier Tamayo de Miguel

María Arrate Muñoz Barrutia

Classroom 7.1.J03, Escuela Politécnica Superior

July 5th 2019, 15:00



This work is licensed under Creative Commons **Attribution – Non Commercial – Non Derivatives**

ABSTRACT

Breast cancer is the most prevalent type of cancer around the world. It has been studied extensively thanks to several immortal cell-lines which have provided accurate and cost-effective models. Their mechanical behavior has been described recently thanks to the new techniques available and a rising interest in biomechanics. In the present study, the stiffness of three cell-lines (two cancerous, MCF-7 and MDA-MB-231, and a healthy one, MCF-10A) have been studied using a digital holographic microscope and osmotic shocks. The latter were achieved by changing the media of the cells from lower to higher concentrations of NaCl. To study their stiffness, the bulk modulus of these three cell lines was calculated by quantifying their deformation using the digital holographic microscope.

ACKNOWLEDGMENTS

My heartfelt thanks to my tutors and supervisors at the Micro and Nanotechnology Institute of the Spanish National Research Council (CSIC) and at the University: Álvaro Cano Tortajada, Marina López Yubero, Priscila Monteiro Kosaka and María Arrate Muñoz Barrutia for giving me the chance to carry this project and helping me with it at every step of the way, providing clear guidance and advice whenever I needed it.

I am also very thankful for my father, mother and sister, for their unconditional support and love, no matter the outcome nor the distance separating us.

I also thank my friends for their help and sympathy whenever motivation and will-power faltered, especially José for his constant words of encouragement.

Table of contents

1. INTRODUCTION	12
1.1 Motivation	12
2. STATE OF THE ART	14
2.1 Holography	16
3. MATERIALS AND RESOURCES	19
3.1 Cellular lines	20
3.1.1 MCF-10A	20
3.1.2 MCF-7	21
3.1.3 MDA-MB-231	22
3.2 Media Preparation	23
3.2.1 Osmosis and osmotic pressure	25
3.2.2 Cell Culture	27
3.3 Refractometry	28
3.4 Digital Holographic Microscopy	30
3.4.1 Principle of DHM	31
3.4.2 Mathematical background	32
3.4.3 Koala software	35
4. EXPERIMENTAL PROCEDURE AND RESULTS	36
4.1 Refractive Index Measurements	36
4.2 Cellular Refractive Indexes	38
4.3 Measurement of the cells' dimensions	40
4.3.1 Media transfusion	40
4.3.2 Phase calculations	41
4.3.3 Volume computations	42
4.4 Bulk Modulus	45
4.4.1 Mathematical background	45
4.4.2 Results of the stiffness study	46
5. DISCUSSION AND IMPLICATIONS OF FUTURE RESEARCH	50
6. CONCLUSION	52

7. SOCIO-ECONOMIC IMPACT	53
7.1 Budget	54
7.1.1 Material cost	54
7.1.2 Labor cost	54
7.1.3 Services cost	55
7.1.4 Overall cost	55
8. REGULATORY FRAMEWORK	56
BIBLIOGRAPHY	57
ANNEX I: ERROR CALCULATIONS	60

List of figures

<i>Figure 1 Experimental techniques for the study of the rheological properties of cancer cells versus normal cells at whole cell scale (left) and local scale (right) [3].</i>	15
<i>Figure 2 First hologram and holographic reconstruction, 1948 [30].</i>	17
<i>Figure 3 Three-dimensional laser hologram of a toy train, recorded by Emmett Leith and Juris Upatnieks. [10]</i>	18
<i>Figure 4 Hologram recording in off-axis transmission, the object is a portrait of Dennis Gabor [11].</i>	18
<i>Figure 5 Workflow of the experiment.</i>	19
<i>Figure 6 MCF-10A Cells.</i>	20
<i>Figure 7 MCF-7 Cells.</i>	21
<i>Figure 8 MDA-MB-231 Cells.</i>	22
<i>Figure 9 Abbe Refractometer 2WAJ. Instituto de Micro y Nanotecnología (CSIC)</i>	28
<i>Figure 10 Screenshot of the technical characteristics of the Abbe Refractometer 2WAJ. [22]</i>	29
<i>Figure 11 Optical set up for transmission DHM [23].</i>	30
<i>Figure 12 Interior of the Lyncée Tec DHM used in this work.</i>	31
<i>Figure 13 The hologram and the three images that are reconstructed from the intensity pattern [24]</i>	33
<i>Figure 14 Koala Software. There are three screens on which the phase reconstruction, the hologram and the Fourier transform of the object are always displayed and monitored during the calculations.</i>	35
<i>Figure 15 View through the Abbe refractometer when measuring the refractive index [26].</i>	36
<i>Figure 16 Ficoll components [32].</i>	38

Figure 17 Segmentation of the one cell (MDA-MB-231) using Matlab function "roipoly"	41
Figure 18 Volume of all three cell-lines at each medium.	43
Figure 19 Left: MDA-MB-231 cells at 0 atm of osmotic pressure; right: same cells, at ~25atm of osmotic pressure.	44
Figure 20 MCF-10A, MCF-7 and MDA-MB-231 Bulk moduli for each medium change.	46
Figure 21 Pressure versus deformation in all three cell lines.	47
Figure 22 Bulk modulus of the three cell lines when switching from Medium 1 to Medium 2. Increase in pressure is $\Delta P=0,65$ MPa.	48
Figure 23 Bulk modulus of the three cell lines when switching from Medium 1 to Medium 3. Increase in pressure is $\Delta P=1,30$ MPa.	48
Figure 24 Bulk modulus of the three cell lines when switching from Medium 1 to Medium 4. Increase in pressure is $\Delta P=1,94$ MPa.	49
Figure 25 Bulk modulus of the three cell lines when switching from Medium 1 to Medium 5. Increase in pressure is $\Delta P=2,62$ MPa.	49

List of tables

<i>Table 1 Composition of the MCF-10A growth medium.</i>	<i>23</i>
<i>Table 2 Composition of the MCF-7 and MDA-MB-231 growth medium.</i>	<i>24</i>
<i>Table 3 Mass of NaCl in each medium. See Annex 1 for the uncertainties.</i>	<i>26</i>
<i>Table 5 Osmotic pressure caused by the concentration of NaCl in each medium. See Annex 1 for the formulas used to compute the errors.</i>	<i>27</i>
<i>Table 6 Refractive indexes of each medium with the Ficoll alternative.</i>	<i>37</i>
<i>Table 7 Refractive indexes of the Media containing NaCl for each cell line.</i>	<i>37</i>
<i>Table 8 Refraction index of each cell line. See Annex 1 for error calculations.</i>	<i>39</i>
<i>Table 9 Dimensional parameters for each cell line.</i>	<i>42</i>
<i>Table 10 Pressure changes from one medium to another. It is important to note that the pressure in MCF-10A medium and MCF-7 and MDA-MB-231 medium are very similar, which means that their bulk modulus will be comparable.</i>	<i>45</i>
<i>Table 1 Labor cost with all taxes included.</i>	<i>54</i>
<i>Table 12 Material cost with all taxes included. * & ** See Table 1 and Table 2 for the exact components.</i>	<i>54</i>
<i>Table 13 Labor cost with all taxes included.</i>	<i>54</i>
<i>Table 14 Services & licenses cost with all taxes included.</i>	<i>55</i>
<i>Table 15 Total cost of the project. Taxes have been included in the subtotals.</i>	<i>55</i>

1. INTRODUCTION

The present work has been carried at the Micro and Nanotechnological Institute of the Spanish National Research Council (CSIC) under the supervision of Álvaro Cano Tortajada and Marina López Yubero.

This thesis is structured in eight chapters: following this introduction is the state of the art, in which past and current tools in cellular nanomechanics are explained; chapter three includes the materials and methods used in this project and, in chapter four, the experimental procedure and the results are shown. The discussion of the results and future lines of work, as well as the conclusion, the socio-economic impact and the regulatory framework are each written in chapters five, six, seven and eight, respectively.

1.1 Motivation

It is estimated that one in six deaths around the world is caused by cancer, breast and prostate cancer in especial as they are the most prevalent type of cancer, according to the Global Health Metrics. The number of patients affected by this disease has more than doubled since 1990, from 45 million people to 100 million patients around the world in 2017 [1]. Cancer is present in all countries, regardless of their development, and across all ages, races and income. This means that the group of diseases under the name of cancer are not restricted to a certain population, but the complete opposite: they affect humanity as a whole.

Nonetheless, the survival rates have also increased since 1990 and patients are able to carry on with a certain quality of life during and after the treatment. This is thanks to the efforts that have been put into facing this challenge and the medical and technological advances achieved by doing so. Since cancer was discovered in 1775 by Percival Pott [2], it has been studied at every level possible, from the inside out, its genomic, the biological and biochemical processes in the tumor cells and, more recently, its biomechanics and physical characteristics have been quantified thanks to the new tools available. One of these tools is Digital Holographic Microscopy, a technique that has allowed a drastic increase in image resolution and phase quantification and is providing promising results in the field of life sciences. Digital holography has been used throughout this work to study the stiffness of cells.

The present work shows the physical and mechanical effects of osmotic shocks carried on both normal (MCF-10A cell line) and cancer cells (MCF-7 and MDA-MB-231 cell lines). The osmotic shock is achieved by washing the cells with increasingly concentrated media (containing NaCl) and thus incrementing the osmotic pressure to which the cells are subjected. Their volume and deformation are measured at each stage using a Digital Holographic Microscope that quantifies the phase changes and can provide information on the thickness (for which the computation of the refractive index is crucial) and the area. This data is finally used to calculate the bulk modulus and compare the three cell-lines' stiffness.

Many studies in the past have demonstrated that cancer cells are more elastic than normal cells through biochemical and even mechanical studies [3]. The objective is to study the stiffness of healthy and cancerous cells by calculating their bulk modulus. Finally, the hypothesis presented in this work is the following: normal cells are stiffer than cancer cells and this may translate into a higher Bulk Modulus for the former and a progressively lower one for the latter the more advanced the cancer is.

2. STATE OF THE ART

The field of biomechanics aims to study the mechanical properties of cells (and the development of tools used for this purpose) at the nanometer level. The objective is to get a better understanding of what happens in biomaterials and living beings beyond the microscopic level, for which many research groups are developing their own devices combining the fields of optics, electronics, mechanics, informatics with medicine and biological sciences. Yuan-Cheng Fung, Professor Emeritus at the University of California San Diego, is considered the “father of modern biomechanics” [4].

The hardness and stiffness of a tumor is misleading when it comes to the study of cellular nanomechanical properties. Many reviews on the matter have hypothesized that cancerous cells are paradoxically softer than their healthy equivalents of the same tissue, but it remains unclear if it is the cells or the stroma that influence the stiffness of the tumor [5-6].

The main difference between cancerous and normal cells is that they grow uncontrollably. They replicate indefinitely by resisting apoptosis (the first programmed death) and growth suppressors by inactivating the genes responsible for tumor suppression [5]. But the most surprising characteristic of cancer is by far its ability to spread through the body. Metastasis is achieved when the cells from a primary tumor detach and create a secondary tumor in an organ significantly far from the former. These cells travel through the body by intravasation and extravasation, meaning that the circulatory system is their means of transport. This process of metastasis is facilitated when the cells are able to efficiently travel through the blood vessels. Therefore, the more deformable they are, the more efficiently they will travel through dense and entangled matrix fibers. Hypothetically, cancer cells' stiffness correlates with their metastatic potential.

On the other hand, it has been shown that cancer cells can move through the body both individually and in cohorts, in which only the first ones may be elastic enough to enter the blood vessels. These cells would be “paving the way” for the following ones [6] to reach their secondary tumor's location, but there is still a possibility that they could encounter a stiffer medium and thus be unable to produce a neoplasm. Therefore, the quantification of cancer cells' stiffness will be useful to increase the knowledge on tumors and their behavior but it will still remain context-dependent.

Despite this, the mechanical characteristics (motility, adhesion and contraction, among others) of tumors as well as their rheological properties have been well-documented. The technological advances are now enabling more accurate measurements of these parameters and a growing number of experimental techniques are being involved in the field of oncology. Some of the ones used to compare healthy and cancerous cells are depicted in Figure 1.

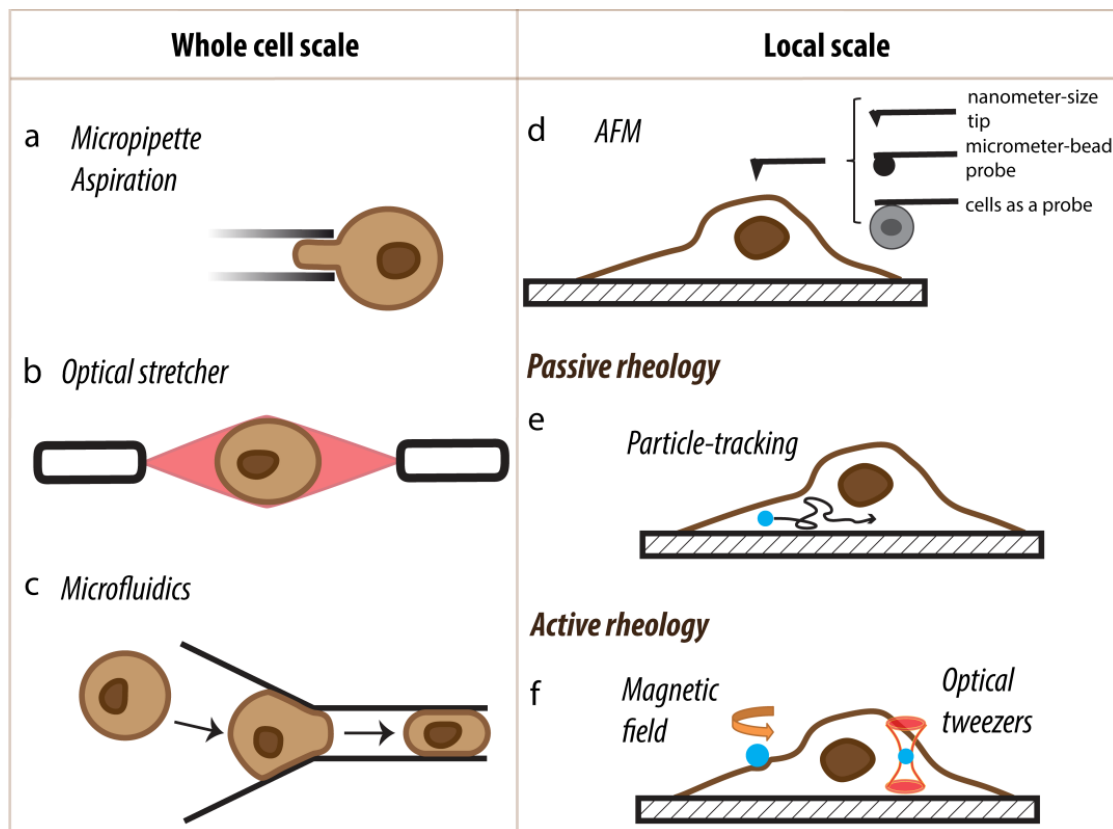


Figure 1 Experimental techniques for the study of the rheological properties of cancer cells versus normal cells at whole cell scale (left) and local scale (right) [3].

Micropipette aspiration (figure 1a): It is one of the earliest techniques to measure cells viscoelastic properties. The cell is suctioned/aspired through a micropipette and the distance it travels through is quantified to define its linearly elastic and creep response.

Optical stretcher (figure 1b): It is a contact-free method that “traps” the cell between two lasers that stretch it. The force that deform the cell is known as the photon momentum which is due to the refraction of photons when they collide with the surface of the cell.

Microfluidics (figure 1c): The cells are forced to flow through channels of a certain geometry, this is by far the most studied technique since it has a myriad of applications.

Atomic Force Microscope (figure 1d): It is a high-resolution type of scanning probe microscopy. A cantilever is placed on the cell and the former's movement is measured. There are many kinds of cantilever depending on the purpose of the experiment. Only local information from cell are obtained.

Particle-tracking (figure 1e): The probe is placed inside the cell and its movement is tracked throughout the cell, but, again, only taking measurements locally from the cell and in a passive fashion since the probe is displaced by the cell itself.

Magnetic field & Optical Tweezers (figure 1f): They both guide the probe inside the cell, through a magnetic force for the former. In the case of optical tweezers, the modus operandi is similar to the optical stretcher, two tightly focused laser beams exert a force on the particle in order to move it.

2.1 Holography

Digital Holographic Microscopy is the technique that has been used in this project. It is a label and contact-free method that allows to take subnanometer accurate measurements of the phase difference introduced in the light's optical path length when it goes through the cells and quantify their dimensions. The history behind this microscope is explained below.

Holography was invented in 1946 by the Hungarian engineer Dennis Gabor (1900-1979) as an attempt to improve the image resolution of electron microscopes, which was 5 armstrongs at the time. His idea of what he called holograms include both the phase and the amplitude of the image taken by a microscope ("*holos*" meaning whole, total), but the procedure and technology to retrieve this information was not fully developed until the 1970's. In 1971 Dennis Gabor received the Nobel Prize in Physics for the development of the holographic theory that allowed him and many other scientists to record the intensity component of the light and obtain the holograms.

The wave-front reconstruction technique developed by Gabor to create a hologram was a two-step process [9]:

1. The two- or three-dimensional object is illuminated with a coherent light, at the beginning it was a mercury lamp with a green filter for monochromaticity and pinholes for spatial coherence, that were later replaced by lasers. The diffraction pattern coming from the object is then recorded on a photographic plate.

2. A raw version of the final image is obtained when the object is removed, and the same photographic plate is illuminated again by the coherent light wave, providing a coherent background for the diffraction pattern to be analyzed.

In his publication [9] he declared that “If a diffraction diagram of an object is taken with coherent illumination, and a coherent background is added to the diffracted wave, the photograph will contain the full information on the modifications which the illuminating wave has suffered in traversing the object”.

The picture of the object is then obtained through the reconstruction of the original wave, using the reference wave. The hologram, as an interference pattern, was first graphically described in two dimensions in 1948 (Figure 2).

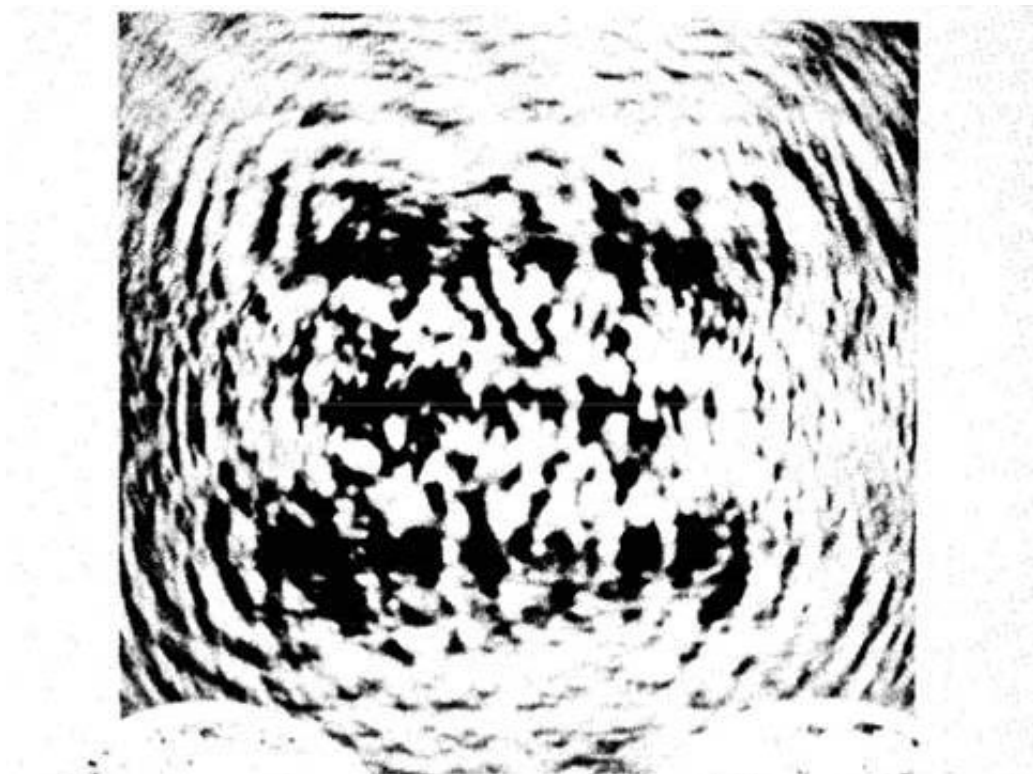


Figure 2 First hologram and holographic reconstruction, 1948 [26]

Gabor and many other physicians and engineers had been working on holographic images for more than a decade when the first three-dimensional high-resolution hologram was registered in 1964 by Emmett Leith and Juris Upatnieks at the University of Michigan. The “Toy Train” picture [10] shown in Figure 3 was obtained thanks to the off-axis set up and a laser, which drastically improved the efficiency of coherent light sources available to researchers.



Figure 3 Three-dimensional laser hologram of a toy train, recorded by Emmett Leith and Juris Upatnieks. [10]

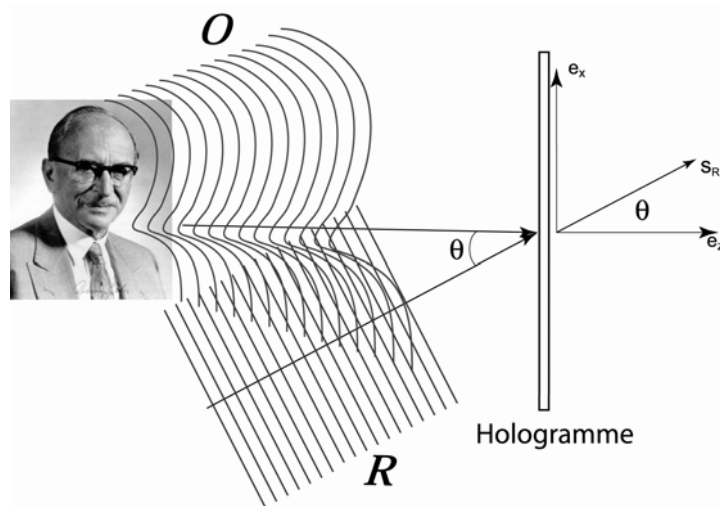


Figure 4 Hologram recording in off-axis transmission, the object is a portrait of Dennis Gabor [11].

In a few words, the off-axis setup is the following: the reference beam and the object beam are coherent beams and they are placed at a certain angle to form the interference pattern, the hologram (“Hologramme” in Figure 4), which is the same operating modes used by current digital holographic microscopes.

Nonetheless, it was not until the very end of the 20th century that holography reached its peak performance with the digitization of the second step of the process. The holograms created by the interference patterns (the object wave) were retrieved by digital cameras, increasing the quality of the final image, and the reference wave was digitally computed. Nowadays, holographic microscopes, specifically Digital Holographic Microscopes, are one of the best non-invasive tools for imaging and used across all industries in a myriad of applications.

3. MATERIALS AND RESOURCES

The “*Equipment and Resources*” chapter begins with a “*Cellular lines*” section on the three types of cells used, followed by a “*Media preparation*” section for a detailed list of the components of the culture media and the effect of NaCl on osmotic pressure. The third section regards “*Refractometry*” in which the refractive index measurements are explained, and the fourth and final section is an introduction to Digital Holography. All the errors regarding the calculations are explained in Annex I.

The workflow of the experiment is explained below. First, the three cell-lines (MCF-10A, MCF-7 and MDA-MB-231) were cultured, and Marina López Yubero provided her knowledge and help for this first step. Different culture plates were used for the refractive index and volume measurements, respectively. For the second step, regarding the refractive index, a refractometer was employed to obtain the index of the media used to wash the cells and alter their mechanical behavior. The index of the cells was calculated by switching from normal media to one containing Ficoll and later analyzing the phase of the cells using the DHM. Finally, the stiffness is a parameter that depends on the volume and pressure, the former is measured with the DHM and the pressure is given by the increasingly higher osmotic pressure from media.

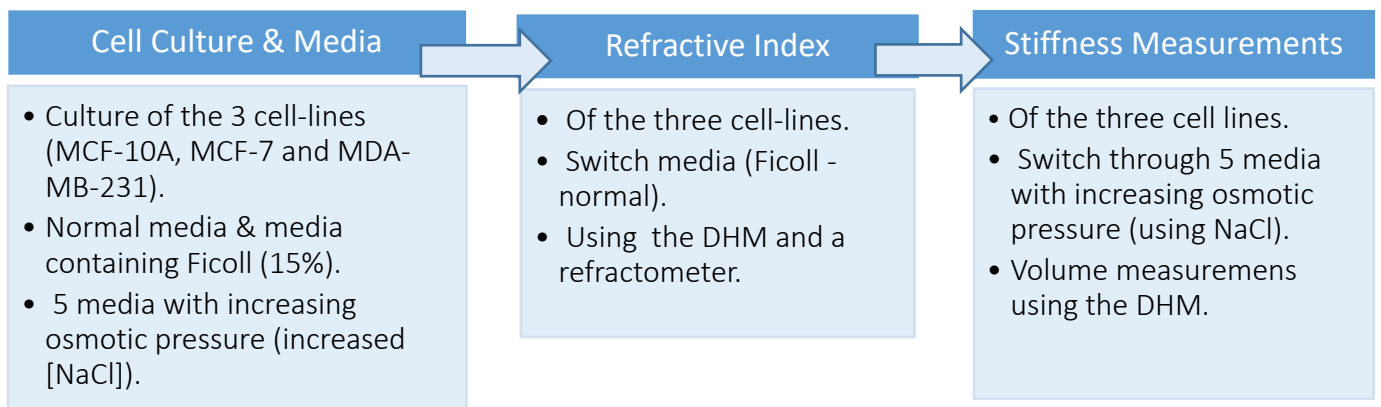


Figure 5 Workflow of the experiment.

3.1 Cellular lines

The MCF-10A, MCF-7, and MDA-MB-231 are the three lines of cells on which the measurements of thickness, volume and refractive index were taken. MCF-7 and MDA-MB-231 cells are cancerous (being MDA-MB-231 the most aggressive), while the MCF-10A come from a healthy patient. These cells have provided accurate models and consistent samples to study biological processes, they are easy to use and a cost-effective alternative to prevent ethical concerns. They were purchased from the American Type Culture Collection (ATCC®, USA) and their characteristics will be explained in the following sections.

3.1.1 MCF-10A

These non-tumorigenic epithelial cells were retrieved from the mammary glands of a 36-year-old patient. They constitute the healthy standard cells of this study. Their characteristics are listed below [12]:

- They can form domes and spread thinly on the culture plates (this is an important behavior, which will deeply affect our calculations, see Figure 6).
- They have a fast-growing phenotype and reach confluency in less than 48 hours.
- They are responsive to insulin, glucocorticoids and epidermal growth factors (EGF).
- They can be grown in three dimensions in collagen.

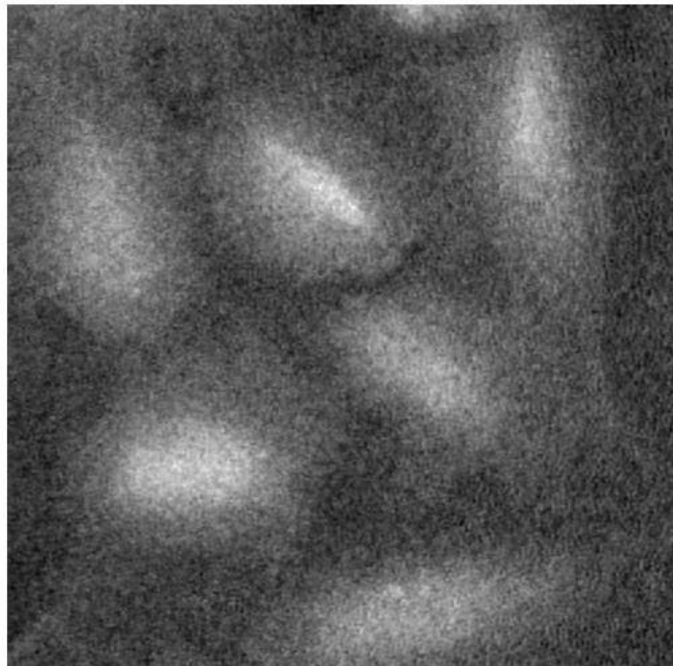


Figure 6 MCF-10A Cells.

3.1.2 MCF-7

This cell-line was extracted from a breast cancer patient in 1970, 69-year-old Sister Catherine Frances (Helen Marion) Mallon. The researcher Herbert D. Soule at the Michigan Cancer Foundation achieved the collection of this cell-line, on which there are currently more than 25 000 publications [13]. Many scientists at the time were trying to immortalize a cell-line to use them as biological models, which had already been achieved with cervical cancer and HeLa cells. MCF-7 stands for Michigan Cancer Foundation (now known as the Barbara Ann Karmanos Cancer Institute) and was Soule's seventh attempt.

The characteristics of MCF-7 cells are listed below:

- They come from the metastasis of a primary tumor: an invasive breast ductal carcinoma that originated from pleural effusion (metastasis) [14].
- They still can form monolayers and dome-like structures when cultured because of the accumulation of fluid between the monolayer and the plate (meaning that they still act like differentiated cells) [13].
- They have estrogen, androgen, progesterone, and glucocorticoid receptors [15]
- They were crucial for the development of estrogen antibodies, which has helped guide the use of hormone therapy in ER-positive tumors [15].
- Many studies have proven that they are tumorigenic in mice [13].
- They are often responsive to chemotherapy [13].

A negative aspect of these cells is that they adapt and evolve over time because of their genomic instability. Nonetheless, they have been used for many genomic studies thanks to their ability to generate an unlimited amount of RNA and DNA [16].

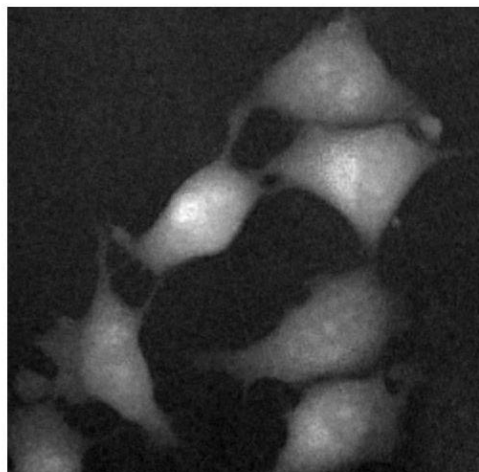


Figure 7 MCF-7 Cells.

3.1.3 MDA-MB-231

MDA-MB-231 cells are also epithelial breast cancer cells, more specifically from the metastasis of an invasive ductal carcinoma (a pleural effusion). They were first isolated in 1973 by R. Cailleau and his collaborators from a 51-year-old female patient in the Anderson Hospital (Houston, USA). The characteristics of these cells are listed below [17-18]:

- They are highly aggressive, invasive and poorly differentiated triple-negative breast cancer cells (TNBC)
- They lack estrogen and progesterone receptors and HER2 (human epidermal growth factor receptor 2) amplification.
- They belong to the Claudin-low molecular subtype because they show a down-regulation of claudin-3 and claudin-4.
- In 3-D cultures they exhibit endothelial-like morphology and is recognized by its invasive phenotype.
- They are not often responsive to chemotherapy.
- They have been established as a tool for bone metastasis research.

MDA-MB-231 cells are highly visible on the DHM throughout the experiment, as shown in Figure 8.

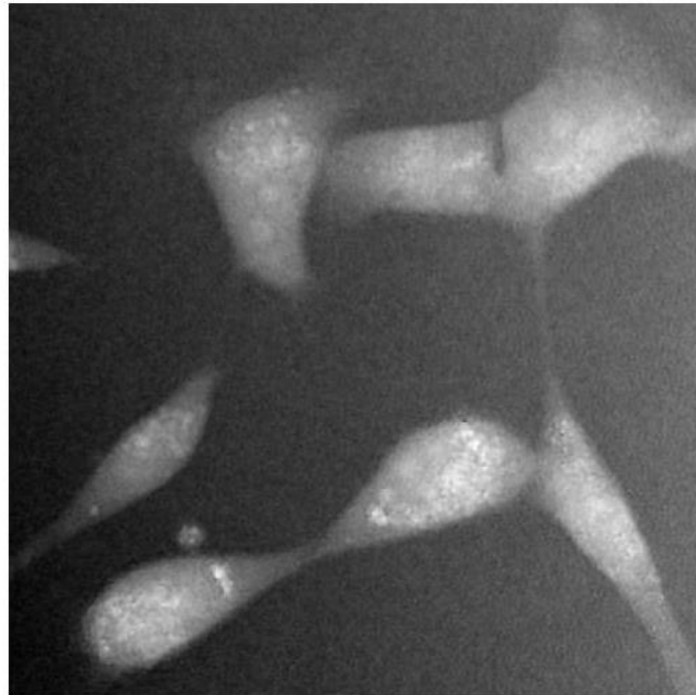


Figure 8 MDA-MB-231 Cells.

3.2 Media Preparation

Cells require a defined set of components in their cell culture media to stay alive and grow on the culture dish. Two different media were prepared for the normal cells (MCF-10A) and the cancerous ones (MCF-7 and MDA-MB-231), respectively. In the following sections, NaCl addition for the creation of osmotic pressure on the cells will be explained.

**MCF-10A
(NORMAL CELLS) GROWTH MEDIUM**

DMEM/F12	500 mL
HORSE SERUM	25 mL
L-GLUTAMINE	5 mL
PEN/STREP	500 μ L
EGF (100MG/ML) LIFE TECHNOLOGIES (PHG0311-100MICROG) (1)	100 μ L
HYDROCORTISONE 1MG/ML (SIGMA H0888-1G) (2)	250 μ g
CHOLERA TOXIN (1MG/1ML) (SIGMA C-8052-1MG) (3)	50 μ L
INSULIN (10MG/ML) (SIGMA I1882-100MG) (4)	500 μ L

Table 2 Composition of the MCF-10A growth medium.

- (1) 100mg of EGF are diluted in 1mL of absolute ETOH. Stored in 100 μ L aliquot at -20°C
- (2) 1mg of Hydrocortisone are diluted in 1mL of absolute ETOH and conserved in 300 μ L aliquots at -20°C
- (3) 1mg of Cholera Toxin is diluted in 1mL of sterile H₂O and are stored in 50 μ L aliquots at -20°C.
- (4) 100mg of insulin are diluted in 10 mL of acid H₂O (a mixture of 10mL of sterile H₂O and 100 μ L of glacial acetic acid). The mixture is store in 500 μ L aliquots and stored at -20°C.

**MCF-7 AND MDA-MB-231
(CANCER CELLS) GROWTH MEDIUM**

DMEM	500 mL
FBS	50 mL
L-GLUTAMINE	5 mL
PEN/STREP	500 μ L

Table 3 Composition of the MCF-7 and MDA-MB-231 growth medium.

MCF-7 and MDA-MB-231 cells are growing continuously and do not require a rich medium to grow. L-glutamine is added because the DMEM did not contain any initially and very little Fetal Bovine Serum is required (FBS). To prevent any infection in the culture dish, a penicillin-streptomycin is included as well.

MCF-10A cells on the other hand require a certain care to remain viable. All the additional ingredients encourage MCF-10A growth, specially the Cholera Toxin, which stimulates the growth of epithelioid cells from normal breast in vitro [19].

All media were stored in a water bath at $\sim 37^{\circ}\text{C}$.

3.2.1 Osmosis and osmotic pressure

When a semipermeable membrane separates two media with different concentrations of solutes, osmosis takes place to restore the equilibrium: water goes from the less concentrated medium to the more concentrated one to dilute it and obtain an equal amount of solute per liter of water in both media. This is what happens at a cellular level: when subjected to a very diluted media, cells tend to absorb as much water as needed to reach equilibrium of concentrations, ending in lysis if the exterior media is highly diluted.

In this work, the opposite phenomenon was used to create a pressure on the cells. The osmotic pressure is the force that prevents water from flowing through the semi-permeable membranes of the cells when equilibrium is reached. During the experiment, each cell dish is exposed to a medium with progressively higher concentrations of NaCl in order to study their mechanical behavior.

A mol of NaCl separates into two moles of active particles (Na^+ and Cl^-), two osmoles that will take part in the osmotic pressure. Therefore, the first step is to compute the effective osmolarity [15] of a certain concentration of NaCl:

$$Osmolarity = \frac{\#Atoms}{Molecule\ of\ solute} \cdot Moles\ of\ solute \cdot \varphi_s \quad 1$$

φ is the osmotic coefficient, a corrective factor of osmolarity, since real solutions are not ideal. The errors eliminated thanks to this coefficient regard the cell membrane behavior and the Na^+ and Cl^- ions interionic attraction that alter the osmotic activity.

The osmotic coefficient is the quantified deviation from Raoult's Law (disregarded in this project), which assumes the perfect behavior of the components of a mixture to compute their partial pressures. The osmotic coefficient calculations based on molarity are described below:

$$\varphi_s = - \frac{\mu_s^* - \mu_s}{RT \ln x_s} \quad 2$$

Where: μ_s^* : Chemical potential of the pure solvent

μ_s : Chemical potential of the solvent in a solution

$$R : \text{Ideal Gas Constant} = 0,082057 \left(\frac{\text{atm} \cdot \text{L}}{\text{mol} \cdot \text{K}} \right)$$

T : Temperature in Kelvin

x_s : Mole fraction

The value of φ_s changes with temperature, concentration and nature of the solute. In the case of solution containing NaCl at body temperature (37 °C) it is $\varphi_s = 0,93$.

Five different media were made for each type of cell (healthy and cancerous): medium 1 contains 0 osmoles of NaCl, medium 2 contains 250 osmoles, medium 3 has 500 osmoles, medium 4 has 750 osmoles and medium 5 contains 1000 osmoles. The corresponding relationship between moles and weight have been calculated and NaCl is weighed on a precision scale in a falcon tube to which the 10mL of media are added using a 5mL pipette. The theoretical and experimental weights are shown below.

Medium	Calculated (mg)	MCF-10A Experimental (mg)	MCF-7 & MDA-MB-231 Experimental (mg)
1	0	0	0
2	78,5	79,000 ± 0,008	78,01 ± 0,01
3	157,1	158,60 ± 0,02	157,20 ± 0,02
4	235,6	238,00 ± 0,02	235,50 ± 0,02
5	314,2	317,00 ± 0,03	319,00 ± 0,03

Table 4 Mass of NaCl in each medium. See Annex 1 for the uncertainties.

The osmotic pressure is the force that prevents water from crossing the semi-permeable membrane to the more concentrated cellular medium. Vant Hoff's law takes into account all the osmotically active particles (osmoles) of solute. In the case of NaCl, a strong salt, the osmotic pressure that it generates in medium of the experiment are shown in Table 5.

The osmotic pressure is described by Van't Hoff's Law [21], derived from thermodynamics.

$$\pi = R \cdot T \sum \varphi_s C_s \quad 3$$

Where: C_s : Concentration of solute $\left(\frac{\text{moles}}{L}\right)$
 R : Ideal Gas Constant = 0,082057 $\left(\frac{\text{atm} \cdot L}{\text{mol} \cdot K}\right)$
 T : Temperature ($^{\circ}K$)

Medium	Calculated (atm)	MCF-10A Experimental (atm)	MCF-7 & MDA-MB-231 Experimental (atm)
1	0	0	0
2	6,4	6,4 ± 0,1	6,3 ± 0,1
3	12,7	12,9 ± 0,2	12,7 ± 0,2
4	19,1	19,3 ± 0,2	19,1 ± 0,3
5	25,5	25,9 ± 0,4	25,7 ± 0,4

Table 5 Osmotic pressure caused by the concentration of NaCl in each medium. See Annex 1 for the formulas used to compute the errors.

For this experiment, the osmotic pressure is a hydrostatic pressure because all the dimensional measurements are taken when equilibrium has been reached, meaning that no net osmosis is happening. Moreover, the greater the amount of water displaced out of the cell to dilute the outside environment, the greater the osmotic pressure. This means that when the outside concentration is increased, the cells suffer a greater osmotic pressure. This pressure becomes hydrostatic when equilibrium is reached.

These unexpected changes in pressure caused by the increment of NaCl in the media that MCF-10A, MCF-7 and MDA-MB-231 will experiment are known as osmotic shocks. Each media increases drastically the osmotic pressure to which the cells are subjected. The whole procedure will be explained in the next chapter.

3.2.2 Cell Culture

All the cell lines were maintained at 37°C and 5% CO₂ humidified incubator. For measuring, cells were plated in 35 mm petri-dishes and grown until the desired confluence. The petri-dish used was a micro-Dish with polymer coverslip bottom that allows high resolution microscopy, as the DHM laser must go through the bottom of the petri dish and provide an accurate phase measurement.

3.3 Refractometry

The refractive index is defined as the quotient of the speed of light in vacuum divided by the speed of light in the medium. It is a dimensionless parameter, symbolized by the letter n :

$$n = \frac{c}{v} \quad 4$$

The smaller the refractive index, the faster light will travel in the medium. The refractive index of light in vacuum is 1,00029 but for practical purposes it is rounded to 1. To quantify this parameter and compare it in different mediums, Snell's formula becomes especially useful:

$$\frac{n_1}{n_2} = \frac{\sin \theta_1}{\sin \theta_2} \quad 5$$

This parameter is especially important for this project because it is crucial to calculate the thickness of each cell and therefore its volume. As light encounters atoms of different nature on its path, it will collide with them, bending to adapt to the new medium.

A tabletop refractometer was employed: Abbe Refractometer 2WAJ. This device has been commercialized for more than 150 years and allows for high resolution measurements of refractive index and sugar content. It comes with a digital thermometer and a water system to ensure the desired temperature on the prism and therefore the samples (see Figure 9), since the refractive index is a temperature dependent parameter.

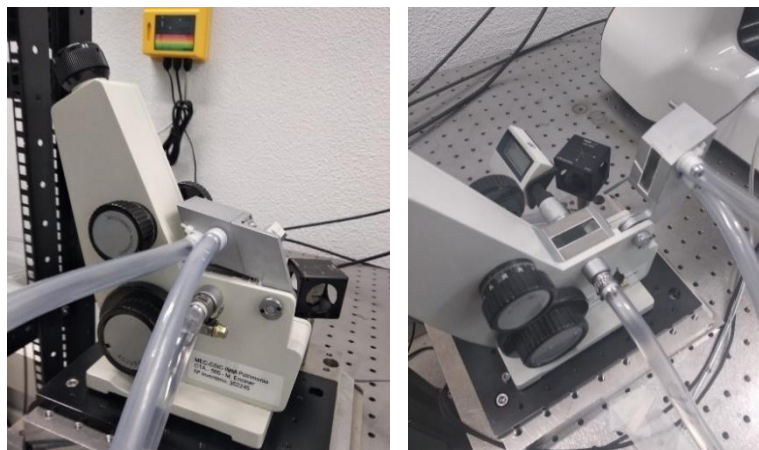


Figure 9 Abbe Refractometer 2WAJ. Instituto de Micro y Nanotecnología (CSIC)

The characteristics chart of the Abbe Refractometer are displayed below.

Model	2W AJ
Refractive Index (nD) Range	1.300 ~ 1.700
Refractive Index (nD) Accuracy	0.0002
Refractive Index (nD) Min. Div.	0.0005
Brix (%) Range	0 ~ 95
Brix (%) Min. Div.	0.25
Weight (KG)	3

Figure 10 Screenshot of the technical characteristics of the Abbe Refractometer 2W AJ. [22]

The refractive index that can be measured by the Abbe Refractometer are between the range of 1,3 and 1,7 with an accuracy of 0,00025.

3.4 Digital Holographic Microscopy

3.4.1 Principle of DHM

The Digital Holographic Microscope (DHM) employed for the experiment was built by Lyncée Tec. It operates with two lasers and provides quantitative phase measurements without using any contrast agents and with very low illumination power on living cellular samples (up to confluence).

The principle of the DHM technology is based on the same off-axis set-up that was first introduced by Leith and Upatnieks. The hologram created by the two coherent beams is collected in a CCD camera with an acquisition time that varies between 1 and 100 microseconds depending on the configuration of the microscopes. This is critical to avoid environmental vibrations and noise and maintain a certain accuracy of the measurements [23].

The DHM used for the experiment was specifically designed for transparent and semitransparent samples since it operates in transmission mode. This means that only the materials and samples that can transmit at least partially the light can form high resolution phase images, otherwise the hologram will be blurry.

In Figure 11 we can see how the holograms are created.

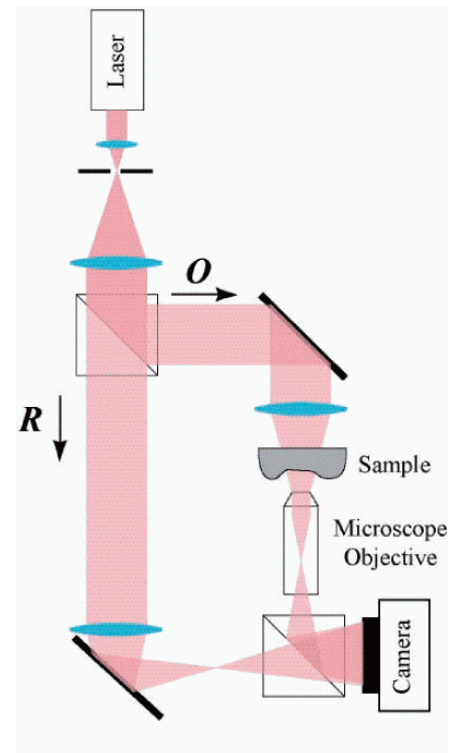


Figure 11 Optical set up for transmission DHM [23].

First, the collimated light source, a laser diode, is separated in two beams: the object beam (**O**), which goes through the sample, and the reference beam (**R**). Both participate in the creation of the hologram by creating an interference pattern, which is collected by the camera. The mirrors are motorized and adjusted by the DHM to maintain the same optical path length for both beams. The **O** wave passes through the sample, while the **R** wave goes directly to the CCD camera.

The optical path length of both **R** and **O** beams must be almost identical for the hologram to be formed. This is crucial because the main goal of the DHM is to quantify the change of phase when the laser goes through the sample, and this can only be achieved if the two beams had the same optical path length originally.

On the other hand, the off-axis set-up (further discussed in the following section) provides the angle difference between the reference beam and the object beam to actually form the interference pattern (the hologram itself).

Finally, to obtain the phase and intensity images from the hologram, the latter must be propagated digitally to the focus plane of the objective. This process is computerized in the case of DHM. Figure 12 below shows the interior of a DHM.



Figure 12 Interior of the Lyncée Tec DHM used in this work.

3.4.2 Mathematical background

To fully analyze all the information provided by a hologram, Lyncée Tec developed a specific software for image processing to obtain the focused phase and intensity images by propagating digitally the hologram to the focus plane of the objective. The mathematics behind it were first explained in a publication from Cucho et al. [24] in which they multiplied a digitally created wave reference by the hologram to obtain a quantitative measurement of the phase.

As mentioned in the previous section, the hologram is formed by the interference pattern of two beams, at the exit of an interferometer. This pattern creates the hologram intensity ($I_H(x, y)$) which is, by definition, the square modulus of the sum of both beam:

$$I_H(x, y) = |R|^2 + |O|^2 + R^*O + O^*R \quad 6$$

R is the reference wave, O is the object wave and R^* and O^* are the complex conjugates of each respective wave.

This hologram is digitized using a CCD camera with pixel size $N \times N = 141 \times 141 \text{ nm}$ and varying size of the image (from $L \times L = 512 \times 512$ pixels to $L \times L = 1024 \times 1024$ pixels, depending on the region of interest that was selected during the experiment). The digitized intensity pattern ($I_H(k, l)$, being k and l the digital substitute of x and y coordinates) is defined by the equation below:

$$I_H(k, l) = I_H(x, y) \text{rect}\left(\frac{x}{L}, \frac{y}{L}\right) \times \sum_k^N \sum_l^N \delta(x - k\Delta x, y - l\Delta y) \quad 7$$

To reconstruct the hologram and the different images we can obtain from it, classical holography re-illuminates the hologram with a replica of the reference wave. In digital holography, this replica is computer-generated using a numerical method, which reproduces the standard procedure of illuminating with the same laser but removing the sample. Multiplying the digital reference wave ($R_D(k, l)$) by the intensity of the hologram, the result obtained is a digitally transmitted wave front (Ψ):

$$\Psi(k\Delta x, l\Delta y) = R_D(k, l) I_H(k, l) = R_D|R|^2 + R_D|O|^2 + R_D R^*O + R_D R O^* \quad 8$$

If it was not digital, the wave front would propagate to the observation plane (the focal plane of the camera), in which we would be able to see three different images of the object:

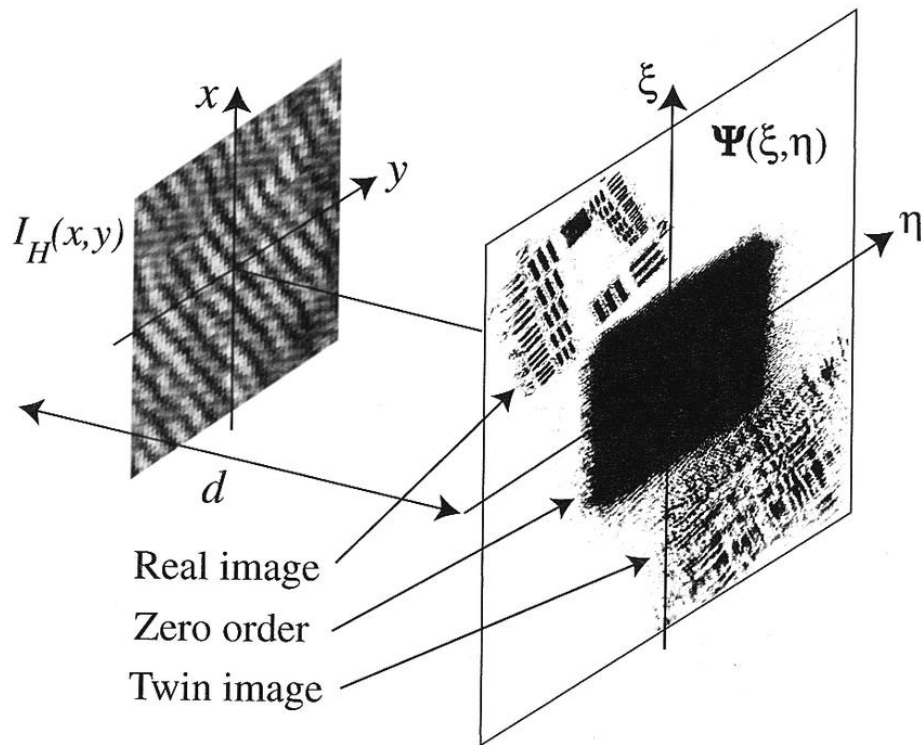


Figure 13 The hologram and the three images that are reconstructed from the intensity pattern [24]

These three images are defined by the terms in the reconstructed wave front formula:

$$\text{Zero Order of Diffraction : } R_D |R|^2 + R_D |O|^2$$

$$\text{Twin Image : } R_D R^* O$$

9

$$\text{Real Image : } R_D R O^*$$

The off-axis setup becomes especially important now that there are three images because the angle difference between the reference beam and the object beam (set by the position of the mirror that reflects the reference beam into the camera) prevents them from superposing each other.

In digital holography, the same three images are created on a computer, thanks to the hologram retrieved from the DHM and the computerized reference wave. Since the wave front is a series of complex numbers, it is possible to quantify the following two images:

- The **amplitude-contrast image**, by calculating its intensity (defined as the square modulus of the sum of the imaginary and real part of a number):

$$I(m, n) = Re[\Psi(m, n)]^2 + Im[\Psi(m, n)]^2 \quad . 10$$

- The **phase-contrast image**, by calculating the argument of the wave front:

$$\Phi(m, n) = \tan^{-1} \left(\frac{Im[\Psi(m, n)]^2}{Re[\Psi(m, n)]^2} \right) \quad 11$$

The phase-contrast one is the image of interest for our calculations. This image is stored in the computer with a pixel size varying between 512x512 to 1024x1024 pixels depending on the region of interest selected (which usually corresponds to the size of the object). The value of each pixel corresponds to the phase.

3.4.3 Koala software

The Koala software is commercialized by the manufacturer Lyncée Tec [25] and sold with the DHM. It was specially designed for the interpretation of the holograms retrieved by the DHM. It is built on C++.net for Windows and allows to make intensity and phase measurements.

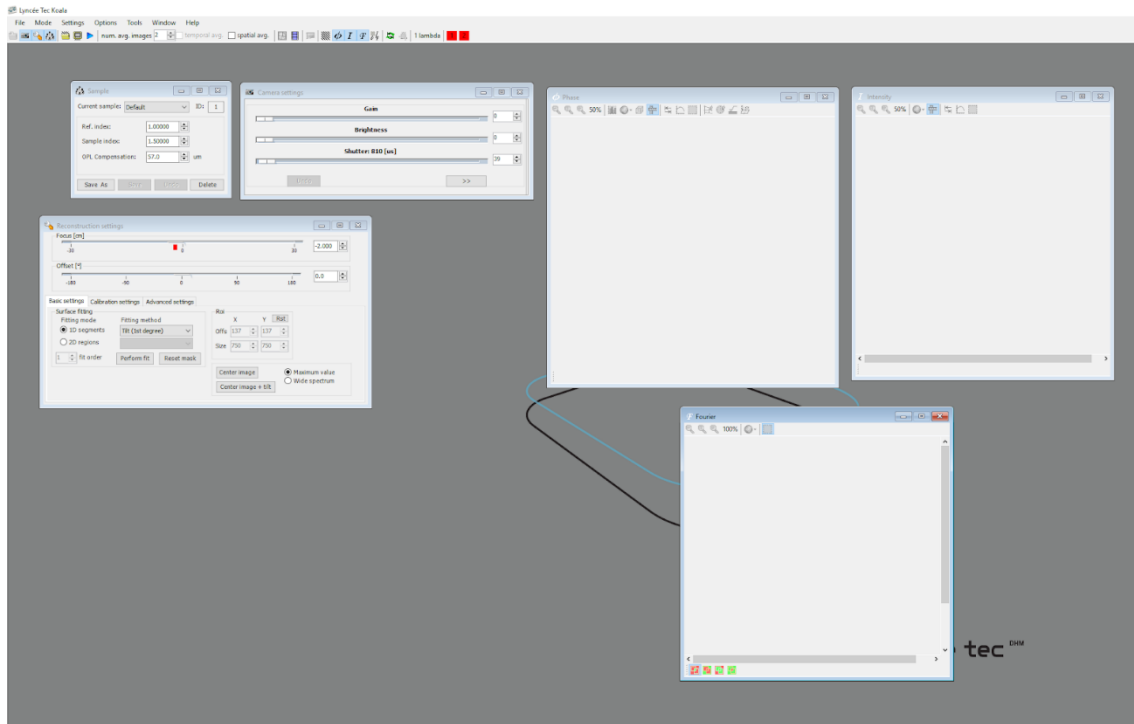


Figure 14 Koala Software. There are three screens on which the phase reconstruction, the hologram and the Fourier transform of the object are always displayed and monitored during the calculations.

This application is especially useful for the reconstruction step, because it allows to perform it long after the sample's hologram has been taken. When reconstructing the image with the numerical method implemented in the Koala software, it is still possible to make some adjustments in exposure time, optical path length and other manual adjustments for example and optimize the algorithm settings for the reconstruction beam. Nonetheless, the camera parameters (such as the exposure time, the optical path length, and the region of interest) cannot be altered since the hologram has already been taken.

4. EXPERIMENTAL PROCEDURE AND RESULTS

In this chapter, the experimental procedure will be explained in detail, presenting the results of each measurement. It begins with the calculation of the media and cell's refractive indexes, followed by the dimensional measurements of the cells using the DHM and finishing with the calculations regarding the bulk modulus of the cells in question. An explanation of the Bulk Modulus measurements has been included in the last sections of this chapter (and not chapter 3) for more coherence and continuity.

4.1 Refractive Index Measurements

The first step is to calibrate the Abbe Refractometer shown in Figure 15 with a standard specimen, such as naphthalene bromide. Then, after cleaning the first substance, the sample is placed on the prism and the refractive index is measured by centering the cross on the bright and dark boundary line (the cross is immobilized). At this point, the value indicated in the green screen below is the index. The laser from the DHM is used to illuminate the sample, by placing a mirror to reflect the laser on the Abbe Refractometer, ensuring that we are using the same red laser ($\lambda=666\text{nm}$) for all the measurements.

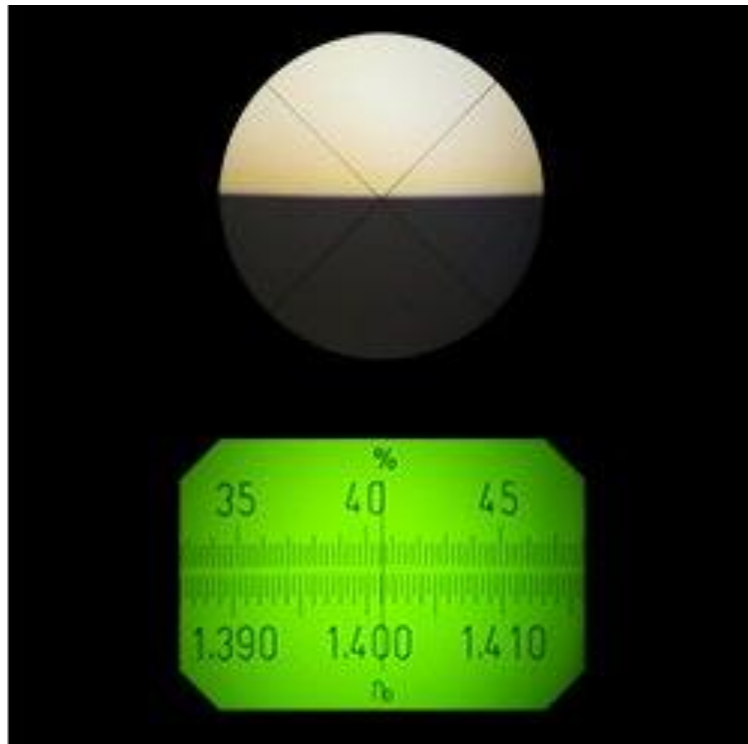


Figure 15 View through the Abbe refractometer when measuring the refractive index [26].

The results for the refractometric measurements for each medium are shown in the tables below.

	MEDIUM	MEDIUM WITH FICOLL
MCF-10A	1,3421 ± 0,00025	1,3693 ± 0,00025
MCF-7 MDA-MB-231	1,3470 ± 0,00025	1,3512 ± 0,00025

Table 6 Refractive indexes of each medium with the Ficoll alternative.

	MEDIUM 1	MEDIUM 2	MEDIUM 3	MEDIUM 4	MEDIUM 5
MCF-10A	1,3415 ± 0,00025	1,3436 ± 0,00025	1,3450 ± 0,00025	1,3475 ± 0,00025	1,3500 ± 0,00025
MCF-7 MDA-MB-231	1,3465 ± 0,00025	1,3480 ± 0,00025	1,3495 ± 0,00025	1,3510 ± 0,00025	1,3375 ± 0,00025

Table 7 Refractive indexes of the Media containing NaCl for each cell line.

4.2 Cellular Refractive Indexes

The refractive index of the cells was obtained through the equation below and the experimental procedure is explained hereunder [27]:

$$\bar{n}_{c,i} = \frac{\delta_n \varphi_{1,i}}{(\varphi_{1,i} - \varphi_{2,i})} + n_{m1} \quad 12$$

Where: $\bar{n}_{c,i}$: integral refractive index for each pixel i

$\varphi_{1,i}$: phase of pixel i from cell in medium 1 (without Ficoll)

$\varphi_{2,i}$: phase of pixel i from cell in medium 2 (with Ficoll)

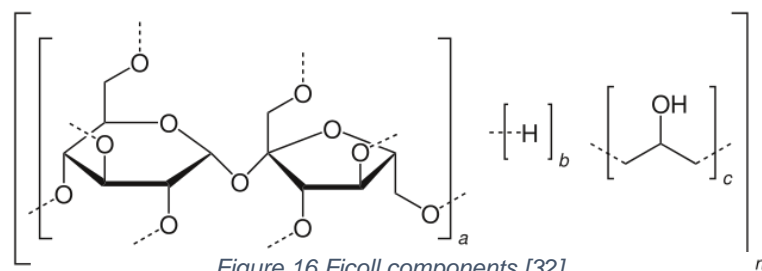
n_{m1} : refractive index of medium 1

n_{m2} : refractive index of medium 2

$$\delta_n = n_{m2} - n_{m1}$$

The phase measurements are taken by the DHM, which have already been explained mathematically in the previous chapter. Since two phases are required to compute the refractive index of each cell, the cell culture was washed with two different media: the first one does not contain any additives and the second one is 15% Ficoll, creating a difference of refractive index.

Ficoll is a highly branched hydrophilic polysaccharide and it is a registered product that belongs to GE Healthcare companies. This substance did not affect the osmolarity of the media and therefore did not generate any change in volume of the cells. It only affected the refractive index of the medium, meaning that we had two media for each type of cell: the normal one (two in total, one for MCF-10A and one for both MCF-7 and MDA-MD-231), and one for Ficoll at 15% (two Ficoll media in total, as well).



Equation 12 computes the integral refractive index for each pixel, but the average pixel value in the cells was used instead. This is especially important when considering the possible errors in the measurements caused by the perfusion of the solution through the petri dish, as the mean average reduces the micro-movement artifacts. The process is described below.

1. The normal media is perfused through the petri dish and it is left to settle for 1 minute approximately.
2. A set of cells are chosen on the DHM (using the Koala software). They will constitute the region of interest.
3. The normal media is removed again and replaced by the second one containing 15% Ficoll. It is left to settle for ~1 minute. The region of interest cannot move since the same set of cells immersed in each media must be compared.
4. A second measurement of the same region is taken.
5. Change the region of interest (the cells visualized) by moving the plate around using the rods of the DHM and repeat the process.

The phase value calculations using Matlab will be explained in the following section.

Since this amount of Ficoll does not affect the cells in any detrimental way, we were able to take measurement for four to five groups of cells per dish, changing the medium as explained, reaching a total 64 cells (21 MCF-7 cells, 21 MCF-10A cell and 22 MDA-MB-231 cells).

The final index of refraction of each cell was computed as the mean value of the measurements taken for each cell line. In the table below, they are compared to water and their respective media's refractive indexes (with their corresponding errors).

MCF-10A	MCF-7	MDA-MB-231
1,382 ± 0,056	1,312 ± 0,015	1,386 ± 0,012

Table 8 Refraction index of each cell line. See Annex 1 for error calculations.

4.3 Measurement of the cells' dimensions

4.3.1 Media transfusion

Five media with different osmolarities are used to generate an osmotic shock in the cells with a pressure ranging from 0 to ~25 atmospheres. The media are transfused through the cells in the petri dishes and left to stabilize and rest until equilibrium has been reached, for ~14 minutes [28], then the phase measurements are taken with the DHM. These petri dishes are placed on the objective of the DHM and their temperature remains at 37,5°C throughout the whole process thanks to the incubator system embedded in the DHM. The first dish is transfused sequentially with the media, from the lowest osmotic pressure to the highest one. This implies that, for each petri dish, only one region of interest containing the same cells was studied while subsequently increasing the osmotic pressure. The media is changed using a pipette while the dish is seating on the objective and watching the cells on the Koala Software to make sure that the region of interest is not moving or compromised. Any cells that disappeared from the ROI during the measurements were discarded and only the ones who had gone through all five media changes were kept. Summarizing:

1. The petri dish is placed on the objective of the DHM and the laser as well as other parameters are calibrated on the Koala Software in order to see the cells clearly.
2. A region of interest is selected: preferably a group of cells clearly separated and visible, with a homogenous background, by moving the rods of the DHM manually.
3. The media present in the petri dish is removed and replaced by the media corresponding to a higher concentration of NaCl.
4. After waiting ~14 minutes [28], 200 holograms are taken, using the Koala Software.
5. Repeat steps 1-4 for each media.

All media and cell dishes were kept at 37°C during the experiment thanks to the incubator embedded in the DHM.

4.3.2 Phase calculations

The mathematical meaning of the phase was discussed in the previous chapter. Experimentally, the phase referred to is the value of each pixel of the phase-contrast images. This value oscillates between $-\pi$ and $+\pi$. The average of the pixel values (phase values) are used to compute the average thickness of the cell, which is the approximation used for this project.

For each region of interest (group of cells visible on the DHM) 200 holograms were taken, subsequently reconstructed to phase-contrast images. The mean image is computed on Matlab and each cell is segmented from it.

The mask for each cell is created using the Matlab function “roipoly”, which allows to create them manually (see Figure 17) and retrieve the average phase of the cell in question (by computing the mean of the pixel value).

Since the phase is a relative parameter and not an absolute value, it was crucial to homogenize them. Therefore, in each image, a region of the background (part of the dish free of cells) was selected and its mean value was subtracted from the average phase value of the cell. This ensured that all the calculations were set to the same scale.

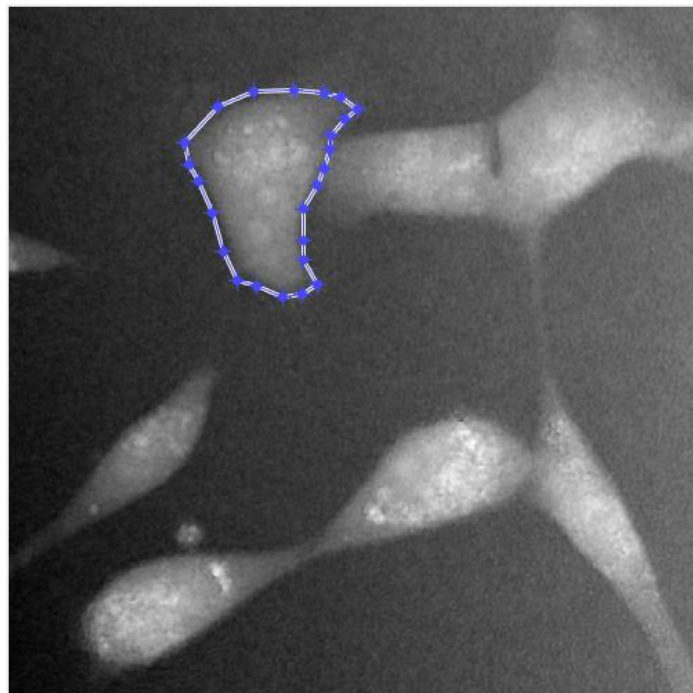


Figure 17 Segmentation of the one cell (MDA-MB-231) using Matlab function "roipoly".

4.3.3 Volume computations

The volume of the cells is calculated as the product of the area by the thickness. This is an estimation; the cells have a complex geometry that make it nearly impossible to compute their volume without using a statistical model. The area is selected manually on Matlab and the thickness is computed using the formula below for each cell:

$$h_i = \frac{\lambda}{2\pi} \frac{\varphi_{1,i}}{(\bar{n}_{c,i} - n_m)} \quad 13$$

$$V = h_i \cdot \text{area} \quad 14$$

Where λ is the wavelength, 666nm in the case of the DHM, the phase $\varphi_{1,i}$ is the average phase of the cell in question, $\bar{n}_{c,i}$ is the refractive index of the cell line (see Table 8) and n_m is the refractive index of the medium (see Table 7). Again, the average thickness of the cell is used instead of making the computations pixel by pixel, to avoid heterogeneities.

Below are the mean dimensional parameters at the beginning of the experiment, when no NaCl has been added.

	MCF-10A	MCF-7	MDA-MB-231
Volume (μm^3)	1850,3 \pm 0,3	3100,4 \pm 0,3	2000,97 \pm 0,3
Area (μm^2)	560,2 \pm 0,1	401,5 \pm 0,1	384,31 \pm 0,1
Thickness (μm)	4,2 \pm 0,3	6,9 \pm 0,3	5,12 \pm 0,3

Table 9 Dimensional parameters for each cell line.

In order to study how the volume changes when NaCl is added, the dispersion of volume of the cells have been plotted in a box chart. The error is given by the standard deviation of the results and shown graphically with the error bars. On the x-axis are the different media. The volume is measured after the cells have spent ~14 minutes in the media.

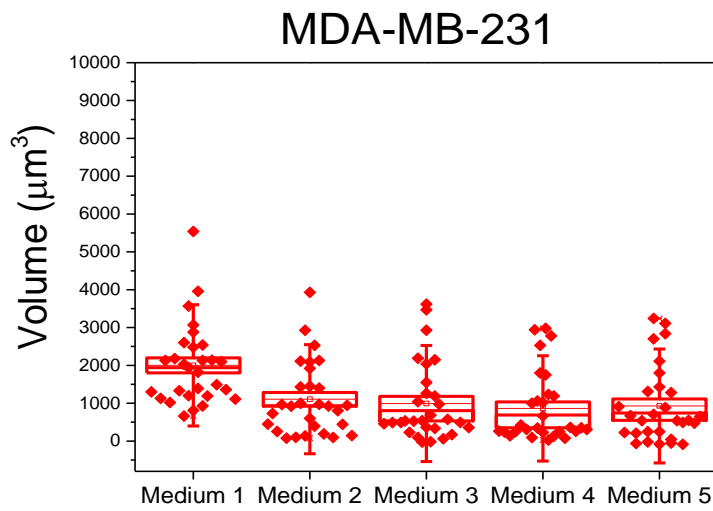
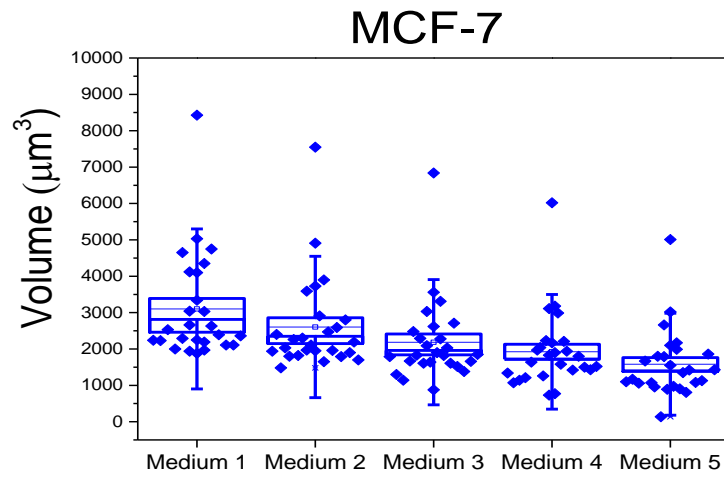
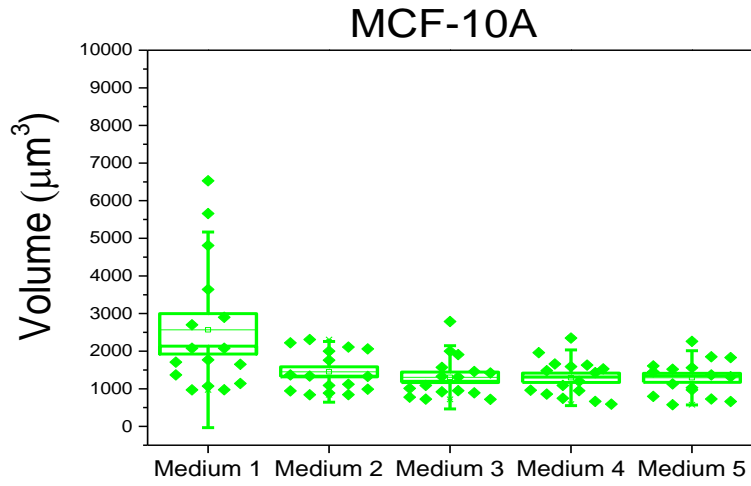


Figure 18 Volume of all three cell-lines at each medium.

From the average values in Table 9 we have seen that the smallest cells in terms of volume are the MDA-MB-231, followed by the MCF-10A and MCF-7; and from the figures, we can see the cells have been quantitatively affected by the osmotic pressure of the media, decreasing their volume. The most drastic changes in volume are observed for the MDA-MB-231 cells, which were also visible to the naked eye (figure 19).

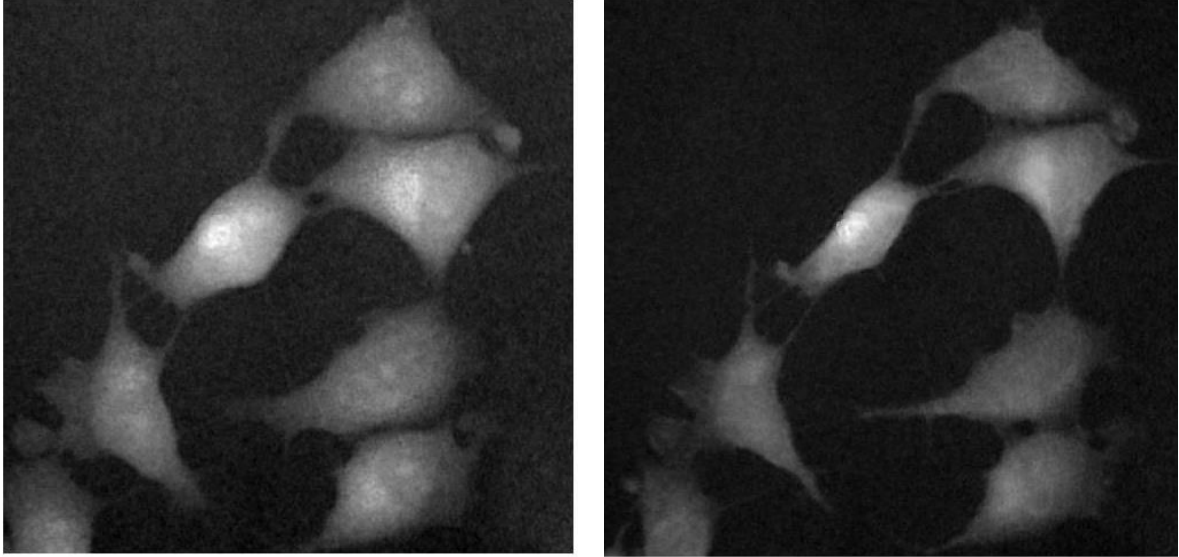


Figure 19 Left: MDA-MB-231 cells at 0 atm of osmotic pressure; right: same cells, at ~ 25 atm of osmotic pressure.

The equation of the thickness (stated at the beginning of this section) depends on the phase. In order to homogenize the measurements, the phase of the cells was calculated with the formula below:

$$\varphi_i = \varphi_{real} - \varphi_{background} \quad 15$$

Where φ_i is the final average phase of the cell taken into account to calculate the thickness; φ_{real} is the average phase of the cell segmented from the phase-contrast image (reconstructed from the hologram taken on the DHM) and $\varphi_{background}$ is the average phase of a region on the background that allowed to make the calculations more accurate by offsetting them and homogenizing them. This is crucial because the cells are compared from medium to medium, meaning that different phase-contrast images of the same cell are compared, and it is important to guarantee that their phases are factually correct for the comparison to be accurate. These calculations of the phase have therefore affected to final measurement of the volume which explains that many of the cells have a volume below average ($< 1000 \mu\text{m}^3$) for the MDA-MB-231 (in red) cells.

4.4 Bulk Modulus

4.4.1 Mathematical background

The Bulk Modulus (B) is the parameter that determines the stiffness of the cells. It quantifies the relationship between an evenly applied pressure and a volume change:

$$B = - \frac{\Delta p}{\left(\frac{\Delta V}{V_o}\right)} \quad 16$$

Where $\Delta p = p_f - p_o$ is the change in hydrostatic pressure (the osmotic pressure in this study) and $\Delta V = V_f - V_o$ is the change in volume, the deformation of the cells. The pressure is hydrostatic meaning that the force applied is the same in all directions. This is the assumption made in this work: the osmotic pressure affects the whole surface of the cell, regardless of the presence of sodium ion channels.

The bulk modulus of a linearly elastic material can be defined by the formula above. Cells, on the other hand, are known to be anisotropic and viscoelastic: they are not homogenous, and they resist the direction of the flow when subjected to a stress system. Therefore, the bulk modulus of the MCF-10A, MCF-7 and MDA-MB-231 cells has initially been calculated without assuming their linearity.

The pressure is measured in Pascals. The osmotic pressured calculated in Table 5 will be recalculated into Pascals (1 atm=101325 Pa) in the table below.

Medium	MCF-10A Experimental (MPa)	MCF-7 & MDA-MB-231 Experimental (MPa)
Medium 1 to 2	0,65 ± 0,01	0,64 ± 0,01
Medium 1 to 3	1,31 ± 0,02	1,29 ± 0,02
Medium 1 to 4	1,95 ± 0,02	1,94 ± 0,03
Medium 1 to 5	2,62 ± 0,04	2,61 ± 0,04

Table 10 Pressure changes from one medium to another. It is important to note that the pressure in MCF-10A medium and MCF-7 and MDA-MB-231 medium are very similar, which means that their bulk modulus will be comparable.

4.4.2 Results of the stiffness study

A total of 16 cells of MCF-10A, 25 cells of MCF-7 and 28 cells of MDA-MB-231 were used in the experiment. The changes in Bulk Modulus for each cell line are shown below.

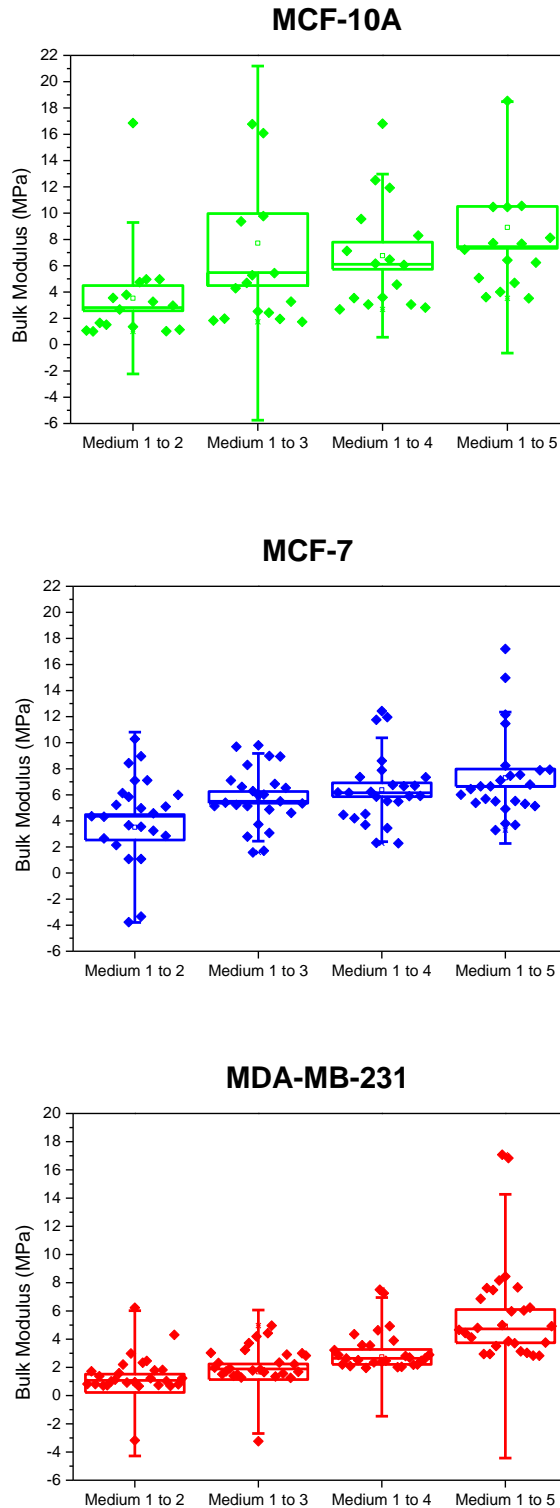


Figure 20 MCF-10A, MCF-7 and MDA-MB-231 Bulk moduli for each medium change.

The error bars shown are calculated from the standard error of the population in question, which is further discussed in Annex I. Regarding the results, the bulk modulus is increasing slightly from medium to medium. The dispersion shows the bulk moduli of the cells (each symbol is a cell) in green for MCF-10A (healthy cells), blue for MCF-7 (the cancerous ones) and red for MDA-MB-231 (the most advanced cancer).

Moreover, the behavior of the three cell lines has shown to be linear when comparing the increase in pressure and the deformation. The figure below depicts this relationship between deformation ($\Delta V/V_0$) and pressure (the bulk modulus is the increase in pressure divided by the relative deformation, which is negative the slope of each plot). The mean average of the deformation is calculated and compared at each stage of the increase in pressure (there is only one data, one symbol, for each increase in pressure, the average is taken, not all the cells). Since the cells are compressed by the osmotic pressure, the final volume is smaller than the initial one ($\Delta V = V_f - V_0$) and therefore $\Delta V < 0$ and all the values on the x axis are negative.

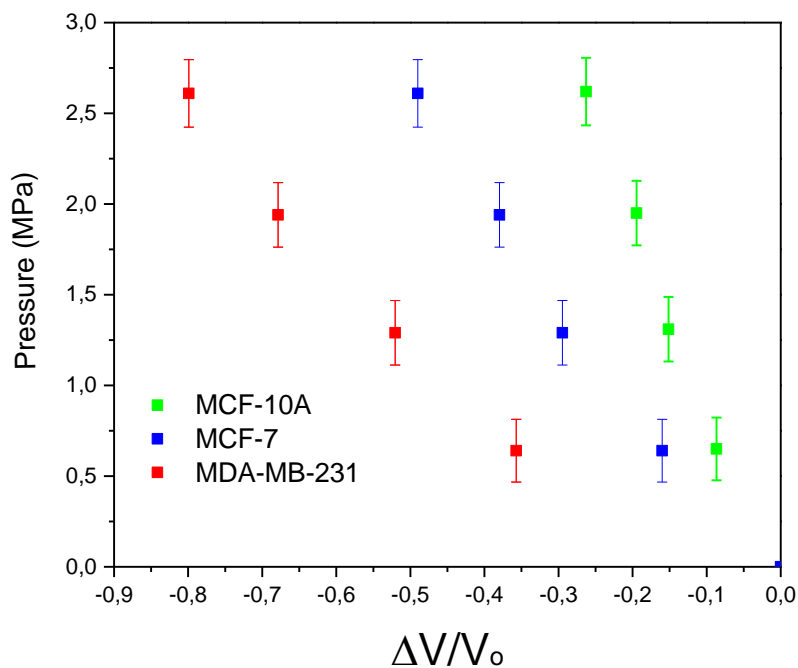


Figure 21 Pressure versus deformation in all three cell lines.

The deformation and increase of volume are compared with reference to medium 1. This means that the increase in deformation is measured with initial volume the volume of the cells in medium 1, and the increase of osmotic pressure starts at 0 because there is no NaCl in the first medium.

Moreover, the plot in Figure 21 shows at first glance that the MCF-10A deform less in comparison with the cancerous cells, being the most deformable the MDA-MB-231 line. The bulk modulus of the three cell lines is compared at each stage (of increase in pressure) in order to get a full vision of their relationship.

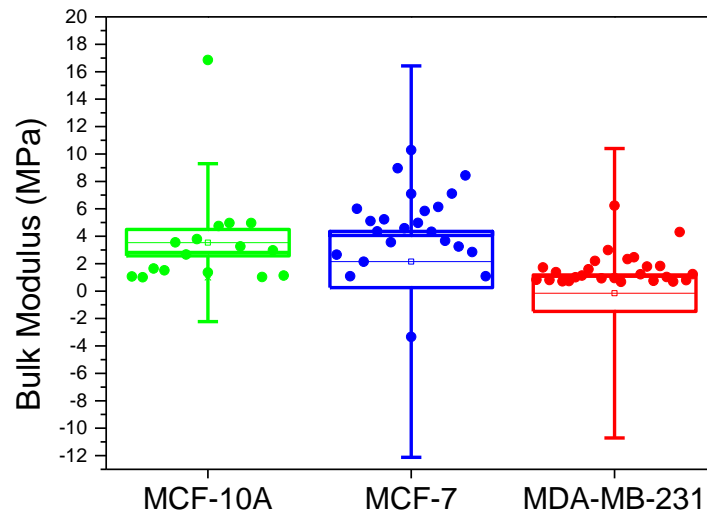


Figure 22 Bulk modulus of the three cell lines when switching from Medium 1 to Medium 2. Increase in pressure is $\Delta P=0,65$ MPa.

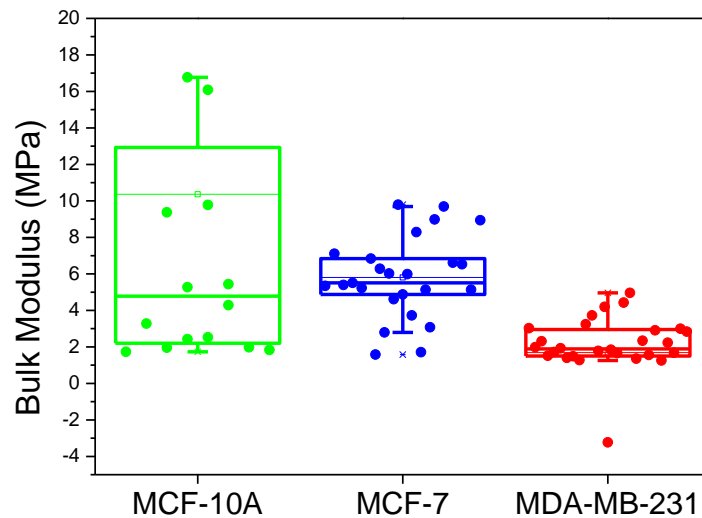


Figure 23 Bulk modulus of the three cell lines when switching from Medium 1 to Medium 3. Increase in pressure is $\Delta P=1,30$ MPa.

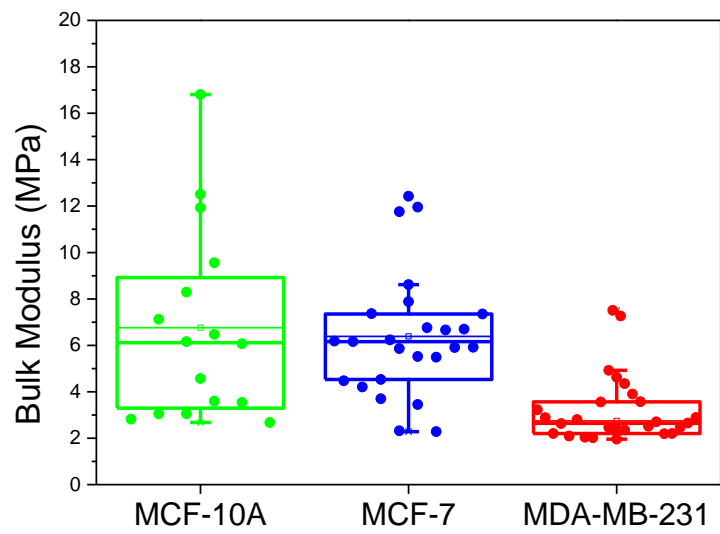


Figure 24 Bulk modulus of the three cell lines when switching from Medium 1 to Medium 4. Increase in pressure is $\Delta P=1,94$ MPa.

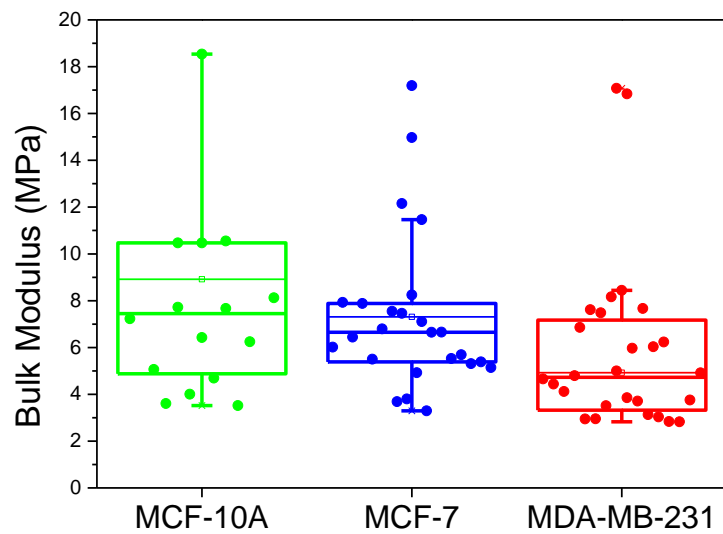


Figure 25 Bulk modulus of the three cell lines when switching from Medium 1 to Medium 5. Increase in pressure is $\Delta P=2,62$ MPa.

Regardless of the osmotic pressure increase, the bulk modulus of the MCF-10A cells remains higher than the cancerous ones and the MDA-MB-231 ones have the lowest bulk modulus.

5. DISCUSSION AND IMPLICATIONS OF FUTURE RESEARCH

The present study has tested the definition of the Bulk Modulus formula to determine the stiffness of normal versus cancer cells using a Digital Holographic Microscope. This is the first time, to the authors knowledge, that digital holography has been used to quantify the rheologic properties of cells. The results and future lines of work are discussed in this section.

The deformation of the cells when subjected to osmotic pressure has been quantified and their behavior has shown to be linear for this experiment, with a clear difference between cell lines. MCF-10A cells have the greatest bulk modulus in comparison with the other two cell-lines, among which the MDA-MB-231 were less stiff than the MCF-7 cells, confirming the initial hypothesis that stiffness and cancer aggressivity are correlated, the more advanced the tumor is, the less stiff its cells will be.

Regarding the conditions of the experiment: while it is true that normal and cancer cells were not exposed to the exact same osmotic pressure, they are very similar, and the error computed may account for this difference. This was mainly due to the weight measurements of NaCl, which was in the order of 100 of mg, making it impossible to adjust exactly to the theoretical quantities displayed in Table 4.

Looking at the box charts more closely, the standard deviation depicted by the whiskers of the box shows that the measurements of MCF-10A are spread across a large range of values, especially when the osmolarity is increased above 500 osmoles (starting from medium 3). This may be due to the dimensions of these cells: they are especially thin in comparison with their cancerous counterparts (see Table 9) and therefore difficult to see on the DHM. The thickness parameter affects the quality of the hologram taken by the DHM and the reconstruction becomes very blurry, since the laser going through the sample is not deviated enough by the cell to create a clear image of the phase change.

Moreover, because of the low quality of the reconstructed images for the MCF-10A cells, they were revised after the segmentation process and compared to the original image again in order to ensure an accurate measurement of the area and thickness, which have been crucial to calculate the Bulk Modulus.

Nonetheless, the hypothesis presented is correct and the normal cells are stiffer than the cancerous ones, the softer one being MDA-MB-231 which belongs to a more advanced cancer than MCF-7.

On the other hand, this study simulated body conditions by performing all the experiments (media and cell refractometry included) at basal temperature ($\sim 37^{\circ}\text{C}$). The main limitation of this experiment is that the cells are adhered on the surface of the petri dish and their cytoskeleton is therefore highly polymerized which means that their mechanical properties are altered [29]. This aspect of the experiment could have been improved if they had been studied in suspension or soft gels had been used in order to mimic the connective tissue environment. However, since a DHM was employed, the phase calculations would have been impossible to perform and get an accurate value of the thickness since the gel would alter all the conditions.

Finally, the mechanical response of these cells when subjected to a stress proved to be highly linear. This assumption cannot be made with all cell-lines, and it is therefore fundamental to first model them accurately. To further study their rheologic properties of these cells, a full cycle of increase and decrease of pressures could have been used to paint an accurate picture of their elastic moduli: by starting with a low concentration of NaCl, rising the pressure to a certain maximum and lowering it again by switching the media to a more diluted one in this case. However, many cells detached or died when the osmotic pressure reached its maximum and therefore this improvement would require a different protocol than the one followed in this experiment.

6. CONCLUSION

By year 2030, cancer will be killing around 13 million people annually, with more than 20 million new diagnostics each year [36]. The use of a DHM to measure the rheological properties of the cells is a new and promising technique that could help us understand their behavior of cancerous versus healthy cells furthermore. The cells' geometry has been approximated with a statistical model and their refractive index has been calculated, which was crucial to compute their bulk modulus.

The hypothesis raised was correct: the cancer cells were softer than normal cells and therefore had a lower bulk modulus. This was achieved by analyzing the volumetric deformation of the MCF-10A (healthy), MCF-7 (breast cancer), MDA-MB-231 (more aggressive breast cancer) cells when subjected to the osmotic pressure of the media (due to the presence of NaCl).

7. SOCIO-ECONOMIC IMPACT

When dealing with a problem, the more knowledge we acquire on a subject, the better equipped we become to solve it successfully, and this is especially important in cancer therapy. Cancer englobes more than a hundred diseases and survival rates are increasing because we have understood that, to cure it, we must be aware of every single genetic anomaly and physical parameters in tumors. Regarding bionanomechanics, this field is very promising in cellular research and this thesis is a very short apercu of the possibilities that exist nowadays.

The initial hypothesis has been confirmed. Cancer cells are more elastic than normal cells and this characteristic could potentially help differentiate between malignant and benign tumors if the techniques are further refined. For instance, by implementing an algorithm for image segmentation, this technique could become time-effective and artificial intelligence could asses the bulk modulus of a group of cells to determine whether they are malignant. This could even erase the labor cost, which is the highest cost, or at least reduce it. The service cost on the other hand drastically increases if the purchase of a DHM is required, since most laboratories don't offer its use. Therefore, the socio-economic impact of this technique for tumor cell's identification is currently negative but this could soon change thanks to the improvement of microscopy techniques used to quantify such parameters.

7.1 Budget

The information regarding the items and services used to carry this experiment are displayed below.

7.1.1 Material cost

Material	Quantity	Total cost (€)
1000µL Pipette	1	30
Pipette tips	160	10
Ibidi petri dishes	25	120
Falcon tubes	12	5
Ficoll	10mL	28
MCF-10A Medium*	100mL	34
MCF-7 & MDA-MB-231 Medium**	100mL	28
NaCl	1 bottle of 100gr	3
MCF-10A Cell culture	1	595
MCF-7 Cell culture	1	595
MDA-MB-231 Cell culture	1	595
	SUBTOTAL	2043 €

Table 11 Material cost with all taxes included. * & ** See Table 2 and Table 3 for the exact components.

7.1.2 Labor cost

Role	Hourly wage (€/h)	Time (hours)	Total cost (€)
Laboratory Technician	7,5	20	150
Scientist for DHM calibration	20	5	100
Junior Biomedical Engineer	6	500	3000
		SUBTOTAL	3150 €

Table 12 Labor cost with all taxes included.

7.1.3 Services cost

Services	Time of Use (hours)	Total cost (€)
DHM Microscope & Koala Software Services	35	1400
Student Matlab License	-	0
OriginLab License	-	560
Laboratory access	40	1000
	SUBTOTAL	2960 €

Table 13 Services & licenses cost with all taxes included.

7.1.4 Overall cost

Concept	Total cost (€)
Material cost	2043
Labor cost	3150
Services cost	2960
Direct cost subtotal	8153 €
Indirect cost (15%)	1222,95
Industrial benefits (6%)	489,18
TOTAL	9865,13

Table 14 Total cost of the project. Taxes have been included in the subtotals.

8. REGULATORY FRAMEWORK

This thesis was carried at the Micro and Nanotechnology Institute of the Spanish National Research Council (CSIC). The CSIC became a State Agency by royal decree in 2007 (RD 1730/2007) and the IMN research center is therefore subjected to the many regulations, of which only the most relevant to this topic will be discussed.

The royal decree 67/2010 regulates the occupation risk prevention program, to which all 67 delegations of the CSIC have subscribed. This means that for any activity carried in these research centers, all members of the center must be aware of the risk prevention protocols and pass a short test after they have read the material provided by the administration to start their activity. Moreover, if this activity takes place in the culture laboratories, a research guide must be provided at the very beginning and according to the royal decree 664/1997, all worker's must be protected from biological products during the activity.

Finally, all three cell lines used in the following experiment have been commercialized and used in research around the world. These cells have been purchased from the American Type Culture Collection (ATCC®, USA) and the regulation regarding the importation and exportation of biological products and samples is regulated by the royal decree 65/2006. This law has improved the paperwork dynamics of the sanitary administration, which is crucial nowadays because many samples as well as reagents are imported from other countries, shortening the waiting time for the shipping as well.

BIBLIOGRAPHY

- [1] P. C. Murray et al., "Global, regional, and national age-sex specific mortality for," *Lancet*, vol. 390, pp. 1151-1210, 2017.
- [2] "Cancer.org," 12 June 2014. [Online]. Available: <https://www.cancer.org/cancer/cancer-basics/history-of-cancer.html>. [Accessed 5 June 2019].
- [3] J. B. Manneville et al., "Are cancer cells really softer than normal cells?," *Biology of the cell*, vol. 109, no. 5, pp. 167-189, 2017.
- [4] G. S. Kassab, "Y.C. "Bert" Fung: The Father of Modern Biomechanics," *Tech Science Press*, vol. 1, no. 1, pp. 5-22, 2004.
- [5] Levental et al., "Matrix crosslinking forces tumor progression by enhancing integrin signaling.," *Cell*, vol. 139, no. 5, pp. 891-906, 25 Nov 2009.
- [6] Y. Lu et al., "ppk23-Dependent Chemosensory Functions Contribute to Courtship Behavior in *Drosophila melanogaster*.,," *PLoS Genet*, vol. 8, no. 3, 2012.
- [7] W. R. Hanahan et al., "Hallmarks of Cancer: The Next Generation.,," *Cell*, vol. 144, pp. 646-74, 2011.
- [8] F. G. Lintz et al., "Basal ganglia output reflects internally-specified movements.,," *eLife*, vol. 5, 2016.
- [9] D. Gabor, "Microscopy by reconstructed wave-fronts," *Proceedings of the Royal Society*, vol. 197, no. 1051, 1949.
- [10] J. Uptanieks et al., Artist, [Art]. Bentley Historical Library, University of Michigan, 1964.
- [11] . C. Emery et al., "Digital Holography Microscopy (DHM): Fast and robust systems for industrial inspection with interferometer resolution," *Proceedings of SPIE - The International Society for Optical Engineering*, 2005.
- [12] "ThermoFisher.com," [Online]. Available: <https://www.thermofisher.com/es/es/home/technical-resources/cell-lines/m/cell-lines-detail-553.html>. [Accessed 27 May 2019].
- [13] A. V. Lee et al., "MCF-7 Cells - Changing the Course of Breast Cancer Research and Care for 45 Years," *Journal of the National Cancer Institute*, vol. 107, no. 7, 2015.

- [14] H. D. Soule et al., "A Human Cell Line From a Pleural Effusion Derived From a Breast Carcinoma," *Journal of the National Cancer Institute*, vol. 51, no. 5, pp. 1409-1416, November 1973.
- [15] K. B. Horwitz et al., "MCF-7; a human breast cancer cell line with estrogen, androgen, progesterone, and glucocorticoid receptors.," *Steroids*, vol. 26, no. 6, p. 785 – 795, 1975.
- [16] A. Vinckevicius et al., "Chromatin immunoprecipitation: advancing analysis of nuclear hormone signaling," *J Mol Endocrinol*, vol. 49, no. 2, p. R113 – R123, 2012.
- [17] R. Cailleau et al., "Long-term human breast carcinoma cell lines of metastatic," *In Vitro*, vol. 14, no. 11, p. 911– 915, 1978.
- [18] R. M. Neve et al, "A collection of breast cancer cell lines for the study of functionally distinct cancer subtypes" *Cancer cell*, vol. 10, pp. 515-27, 2007.
- [19] "LGCStandards-ATCC.org," [Online]. Available: http://www.lgcstandards-atcc.org/Global/FAQs/C/C/Cholera%20toxin-541.aspx?geo_country=es. [Accessed 27 May 2019].
- [20] J. E. Hall, Guyton and Hall Textbook of Medical Physiology, 13 ed., Saunders Title, 2016, pp. 259-263.
- [21] J. Feher, "2.7 - Osmosis and Osmotic Pressure," in *Quantitative Human Physiology*, Academic Press, 2012, pp. 141-152.
- [22] Instruction Manual Abbe Refractometer. [Online] Available: https://www.testers.co.uk/downloads/dl/file/id/3268/product/15549/kern_ort_1rs_abbe_analogue_refractometer_user_manual.pdf
- [23] M. P. Emery et al., "Digital Holographic Microscopy (DHM): 3D Real-Time Optical Imaging at the Nanometer Scale," *Imaging & Microscopy*, no. 8, pp. 46-48, 2006.
- [24] C. Cuche et al., "Simultaneous amplitude-contrast and quantitative phase-contrast microscopy by numerical reconstruction of Fresnel off-axis holograms.," *Applied optics*, no. 38, pp. 6994-7001, 2000.
- [25] "<https://www.LynceeTec.com>," [Online]. Available: <https://www.lynceetec.com/koala-acquisition-analysis/>. [Accessed 6 June 2019].
- [26] "Industrial-needs.com," [Online]. Available: <https://www.industrial-needs.com/technical-data/refractometer-abbe-2waj.htm>. [Accessed 27 May 2019].
- [27] B. Rappaz et al., "Measurement of the integral refractive index and dynamic cell morphometry of living cells with digital holographic microscopy," vol. 13, no. 23,

pp. 9361-9373, 2005. Available:

<http://www.giordanostefano.it/file/notes/Dispensa-elasticita-finita.pdf>.

- [28] D. Béatrice Rouzair-Dubois et al., "Relationship between extracellular osmolarity, NaCl concentration and cell volume in rat glioma cells.," *General Physiology and Biophysics*, vol. 30, no. 2, p. 162–166, 2011.
- [29] Q. S. Li, G. Y. H. Lee, C. N. Ong and C. T. Lim, "AFM indentation study of breast cancer cells," *Biochemical and Biophysical Research Communications*, vol. 374, no. 4, pp. 609-613, 2008.
- [30] D. Gabor, "Nobel Lecture: Holography," 1970. [Online]. Available: <https://www.nobelprize.org/prizes/physics/1971/gabor/lecture/>.
- [31] "Optique-Ingenieur.org," 2013. [Online]. Available: http://www.optique-ingenieur.org/en/courses/OPI_ang_M02_C10/co/Contenu.html.
- [32] "Wikipedia.org," [Online]. Available: <https://en.wikipedia.org/wiki/Ficoll>. [Accessed May 27 2019].
- [33] A. K. Ofek et al., "In situ mechanical properties of the chondrocyte cytoplasm and nucleus," *Journal of biomechanics*, vol. 42, no. 7, p. 873–877, 2009.
- [34] M. Chen et al., "Cell mechanics, structure, and function are regulated by the stiffness of the three-dimensional microenvironment," *Biophysical Journal*, vol. 103, no. 6, p. 1188–1197, 2012.
- [35] S. Giordano, "Continuum Mechanics and Non-linear Elasticity," [Online]. [Accessed June 2019].
- [36] American Cancer Society 2015 *Global Cancer Facts and Figures* 3rd edn (Atlanta, GA: American Cancer Society).

ANNEX I: ERROR CALCULATIONS

Three types of uncertainties have affected the calculations carried for this experiment:

- Precision error (ε_p): it is the smallest value measurable in digital devices. For analog instruments $\varepsilon_p = \frac{1}{2} \cdot (\text{smallest value on the scale})$.
- Systematic error (ε_s): it includes instrumental, method and operator error, which offset the measurements due to inaccurate manipulation of the device or poor calibration.
- Random error: errors of stochastic nature that depend on the environmental conditions in this experiment. It has been defined as the statistical error in this work using the formula $\varepsilon_r = \frac{\sigma}{\sqrt{n}}$, being σ the standard deviation of the population and n the total of cells.

All the measurements involving the above errors are gathered in the following table.

Measurement	Type of error	Chapter/Section
Index of refraction using Abbe Refractometer	Precision & systematic	4.1 Refractometry
Weight measurements on laboratory scale; volume for media preparation and pressure calculations	Precision, systematic & random	3.2 Media Preparation
Segmentation of the cells on Matlab, refractive index and thickness measurements of the cells	Systematic & random	4.2 and 4.3
Volume and bulk modulus	Systematic & random	4.3 and 4.4

All the measurements carry a systematic error because of the operator, which was the same person during the whole experiment.

The precision error of the Abbe Refractometer is stated below. It is a unit-less parameter.

$$\varepsilon_{p,refractometry} = \frac{1}{2} \cdot \text{smallest value} = \frac{1}{2} \cdot 0,005 = 0,00025 \quad 1$$

The weight measurements were taken on a laboratory scale with $\varepsilon_p = 0,0001$ grams. Since the measurements were of the order of 50-300 mg, it was difficult to place the

exact weight in the falcon tube. These errors have been quantified by using the equation below:

$$\varepsilon_{weight} = \varepsilon_p \cdot Measurement \quad 2$$

Where the measurement is the amount of NaCl weighted, the greater the weight, the greater the errors because it becomes harder to manipulate the substance and select the exact number of grains required to reach a certain weight. These errors are rounded to one significant digit.

The errors belonging to the media preparation have been reduced to an analog error that depends on the pipette used. In this case, a 5mL pipette with 0,05 mL precision was employed, reducing the error to:

$$\varepsilon_{media} = \frac{1}{2} \cdot smallest\ value = 0,025\ mL \quad 3$$

The error of the weight and the media propagate to the calculations of the osmotic pressure error:

$$\varepsilon_{\pi} = \Delta T \cdot \frac{\partial \pi}{\partial T} + \Delta C \cdot \frac{\partial \pi}{\partial C} = \Delta T \cdot (RC) + \Delta C \cdot (RT) \quad 4$$

Since $\pi=RTC$, where R is the gas constant, T is the temperature and C is the osmolarity, for each medium. ΔT is the temperature precision error ($\pm 0,01^{\circ}\text{C}$) and ΔC is the concentration error and depends on the weight and media errors explained above.

In the segmentation process on Matlab, the pixel size is in the order of nanometers (145 nm to be exact). But on the screen, it was not possible to zoom in and segment the cells with pixel precision, meaning that both operator and systematic error were made. These have been quantified by calculating the random error present:

$$\varepsilon_r = \frac{\sigma}{\sqrt{n}} \quad 5$$

The standard deviation is calculated from $\sigma = \sqrt{\frac{\sum(x_i - \bar{x})^2}{n}}$, where x_i is the cell (one by one), \bar{x} is the mean average and n is the total number of cells. This error was calculated for each group of cells belonging to the same cell line for each change in medium that affected their volume and bulk moduli.